Mineralogical Magazine, October 2006, Vol. 70(5), pp. 463–484

Apatite-group minerals from nepheline syenite, Pilansberg alkaline complex, South Africa

R. P. LIFEROVICH AND R. H. MITCHELL*

Department of Geology, Lakehead University, 955 Oliver Road, Thunder Bay, Ontario, Canada P7B 5E1

ABSTRACT

The nepheline syenites of the Pilansberg alkaline complex (South Africa) have undergone extensive subsolidus equilibration and alteration with a deuteric Cl- and Na-rich fluid phase. Complex assemblages of secondary minerals result from the replacement of primary aluminosilicates, rinkite, eudialyte and fluorapatite. The composition of apatite group minerals formed during these alteration processes reflects the Sr- and rare earth element (*REE*) content, Na/Cl ratio and pH of the deuteric fluids. Apatite-group minerals are observed to have formed in the following sequence: orthomagmatic fluorapatite; strontian britholite-(Ce); strontian fluorapatite; Sr-apatite; *REE*-rich Sr-apatite; Sr-Na-*REE*-rich minerals approaching the stoichiometry of belovite-(Ce) and deloneite-(Ce); britholite-(Ce). Increasing alkalinity of the deuteric fluids is reflected by increasing amounts of Sr replacing Ca in apatite and culminates in the formation of Sr apatite containing 62.1 wt.% SrO (~4.17 a.p.f.u. Sr). Pilansberg apatite-group minerals form a near-complete solid solution between fluorapatite and a fluorine analogue of Sr apatite with limited solution towards belovite-(Ce), Si-rich belovite-(Ce) and strontian britholite-(Ce).

KEYWORDS: lujavrite, foyaite, hyperagpaitic, subsolidus, alteration, strontian, Sr-apatite, britholite-(Ce), belovite-(Ce), Pilansberg.

Introduction

APATITE is a common accessory phase in igneous and metamorphic rocks. Silica-undersaturated igneous rocks, especially nepheline syenite, carbonatite and alkaline ultramafites, are known to host significant economic deposits of apatite. Generally, orthomagmatic apatite approaches the stoichiometry of fluorapatite, $^{IX}Ca(1)_2{}^{VII}Ca(2)_3(PO_4)_3(F,OH)$. Due to the tolerance of the structure for substitutions involving a wide range of cations and anions, apatite-group minerals commonly serve as a sink for incompatible and volatile elements in late-magmatic, pegmatite and postmagmatic mineral parageneses. These substitutions give rise to less common varieties of apatite and apatite-group minerals, enriched in Na, Sr, light rare earth elements (*LREE*), actinides (mostly Th), and Si. High concentrations of these elements are known to induce a series of compositionally-driven phase transitions from $P6_3/m$-structured apatite and strontian fluorapatite to $P6_3$-structured Sr-apatite and fluorcaphite, $P\bar{3}$-structured belovite-(Ce) and belovite-(La), or to $P3$-structured deloneite-(Ce) (Pekov *et al.*, 1995; Khomyakov *et al.*, 1996; Chakhmouradian *et al.*, 2005). The mechanisms of atomic substitutions in natural and synthetic apatite are reviewed in detail by Pan and Fleet (2002).

Compositional variations of the apatite-group minerals provide insights into the evolution of their parental magmas and fluids. In this paper, we describe the textural and compositional evolution of apatite-group and related minerals from nepheline syenites of the Pilansberg peralkaline complex (South Africa).

* E-mail: rmitchel@lakeheadu.ca
DOI: 10.1180/0026461067050346

Geological setting

The Pilansberg complex is a large differentiated intrusion of nepheline syenite, tinguaite and associated alkaline volcanic rocks (Shand, 1928). The complex is a partially-unroofed ring structure ~25 km in diameter (Fig. 1). It was emplaced at a contact between granitic and noritic units of the Bushveld complex, during the Middle Proterozoic (Retief, 1963). The complex has been little studied, the only significant works being those of Shand (1928), Retief (1962, 1963), Ferguson (1973) and Lurie (1986). Previous studies have demonstrated that extensive autometasomatic processes have affected the nepheline syenite (Lurie, 1986; Mitchell and Liferovich, 2004, 2005, 2006).

In general, the complex consists of large arcuate intrusions of 'red', 'white', and 'green foyaites' (Shand, 1928), 'Ledig foyaite' (Lurie, 1986) and tinguaite dykes and cone sheets (Fig. 1). These nepheline syenites are similar to lujavrite, khibinite and foyaite occurring in the Khibina, Lovozero, Poços de Caldas, Ilímaussaq and North Qôroq peralkaline complexes.

The 'green foyaite' consists of discontinuous arcuate units. Flow-alignment of alkali feldspar, albite and aegirine phenocrysts imparts a foliated trachytic texture (Fig. 2*a*), identical to that of type-locality lujavrite at Lovozero (Ramsay, 1890; Féménias *et al.*, 2005). All of the 'green foyaites' which consist of alkali feldspar, albite, nepheline, sodalite, aegirine, eudialyte and sodic amphibole as primary minerals, are termed lujavrite in this work, regardless of their texture. The major varieties of lujavrite are fluidal, porphyritic and inequigranular trachytic-to-massive (Fig. 2*a*–*d*). Detailed descriptions of these lujavrites are given by Mitchell and Liferovich (2004, 2005, 2006). Astrophyllite, rinkite and lamprophyllite are orthomagmatic accessories in lujavrite, which has an agpaitic index of 1.30–1.35 (Shand, 1928; Olivo and Williams-Jones, 1999). A fluidal aegirine-rich

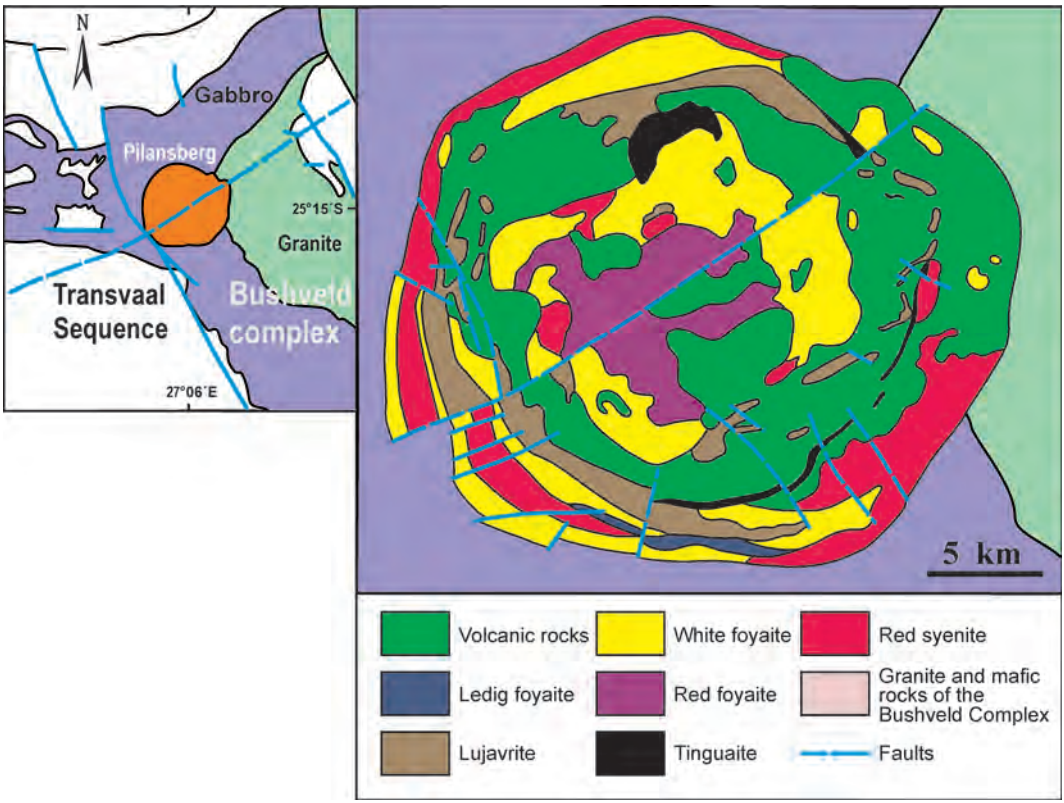

FIG. 1. Generalized map of the Pilansberg peralkaline Complex (after Shand, 1928 and Lurie, 1986).

melanocratic variety of lujavrite (melanolujavrite, Fig. 2*b*) has an agpaitic index of 1.79 (Shand, 1928) and thus is a 'hyperagpaitic' rock (Khomyakov, 1995).

White foyaite is equigranular and relatively uniform in mode, although textures transitional to trachytic are commonly found. Alkali feldspars, nepheline, sodalite, sodic amphibole, and aegirine-augite are the major minerals with cancrinite, biotite, albite, rinkite, eudialyte, apatite, strontianite and fluorite as minor phases (Fig. 2*e*,*h*). 'Ledig foyaite' is an albite-rich, meso-to-melanocratic nepheline syenite with abundant spherules of green acicular aegirine measuring a few millimetres in diameter (Fig. 2*f*). 'Ledig foyaite' is the youngest of the Pilansberg nepheline syenites (Lurie, 1986).

Extensive studies based on optical and back-scattered electron petrography demonstrates that all Pilansberg nepheline syenites have experienced multistage aometasomatic alteration, similar to that described for the lujavrite (Mitchell and Liferovich, 2004, 2006). In general, the stages of alteration were: (1) early-postmagmatic alteration of sodalite and eudialyte-I characterized by formation of an early 'miaskitic' paragenesis during low alkalinity conditions; (2) re-crystallization of K-feldspar and conversion of nepheline to analcime with formation of 'agpaitic' and then 'hyperagpaitic' mineralization during increasing alkalinity; and (3) recurrent agpaitic; and (4) latest miaskitic assemblages.

Paragenesis of the apatite-group minerals

Apatite-group minerals were formed during late- and post-magmatic evolution of nepheline syenite. Textural relationships with other minerals permit the recognition of several generations of apatite-group minerals. These can occur independently, occupy interstices between aegirine crystals (Fig. 3*a*), and more commonly as complex overgrowths (Fig. 3*b*–*d*), and products of alteration of earlier-forming minerals (Figs 2*g*,*h* and 3*d*–*h*).

Orthomagmatic fluorapatite (referred to hereafter as FAp) occurs as euhedral prismatic crystals in a paragenesis with nepheline, aegirine-augite, early poikilitic eudialyte-I, rinkite, and astrophyllite. Fluorapatite in sodalite-rich white foyaite commonly shows anomalous interference colours (Fig. 2*h*) and is enriched in Si and *LREE* (referred to hereafter as FAp-*LREE*). Together with eudialyte-I (Mitchell and Liferovich, 2006) and other orthomagmatic minerals, FAp has undergone extensive postmagmatic alteration and is typically found as strongly corroded relics, within aggregates of later-forming apatite-group minerals (Fig. 3*c*).

The earliest post-magmatic phase to form was britholite-I (referred to hereafter as Brt-I), replacing rinkite, eudialyte and fluorapatite (Fig. 2*g*,*h*) at the stage of sodalite-to-analcime conversion and decomposition of orthomagmatic eudialyte (eudialyte-I of Mitchell and Liferovich, 2006). Brt-I occurs in the early 'miaskitic' paragenesis together with zircon, pyrochlore, allanite and fergusonite. In some instances, reaction of apatite with fluid, together with formation of Brt-I pseudomorphs gave rise to a consanguineous Ca-Na zeolite (probably, gonnardite) mantling FAp/Brt-I aggregates (Fig. 2*h*).

Strontian fluorapatite (referred to hereafter as FAp-Sr) is widespread in all Pilansberg nepheline syenites and has crystallized at relatively high alkalinity in a paragenesis with the late generation of euhedral strontian eudialyte (eudialyte-II of Mitchell and Liferovich, 2006) and lamprophyllite-group minerals. FAp-Sr replaces and mantles previously-formed FAp and Brt-I (Fig. 3*c*,*d*) and, in turn, has been subjected to alteration to exotic apatite-group minerals at the contacts with analcime and natrolite.

Sr-apatite (referred to hereafter as SrAp) crystallized during conditions of maximum alkalinity, marked by the destabilization of precursor 'miaskitic' and 'agpaitic' minerals, e.g. by replacement of eudialyte by sodic zirconosilicate (Mitchell and Liferovich, 2004, 2006). Sr-apatite occurs in association with analcime, catapleiite-like sodic zirconosilicate(s), lamprophyllite-group minerals, acicular aegirine, stronalsite, serandite and diverse unidentified sodic phases (Mitchell and Liferovich, 2004, 2006). In lujavrite, SrAp commonly occurs in aggregates replacing euhedral crystals of eudialyte-II, but has not been recognized in Ledig and white foyaites. Both corrosional relationships and epitaxial overgrowths are observed between precursor apatite-group minerals and SrAp. In most instances, the latter mantles FAp-Sr or forms discontinuous rims (Fig. 3*c*). In some instances, SrAp forms complete pseudomorphs after precursor apatite-group minerals enclosed in prismatic aegirine-augite (Fig. 3*f*). SrAp also appears as isolated grains occupying interstices in aggregates of acicular aegirine or as granular clusters in analcime.

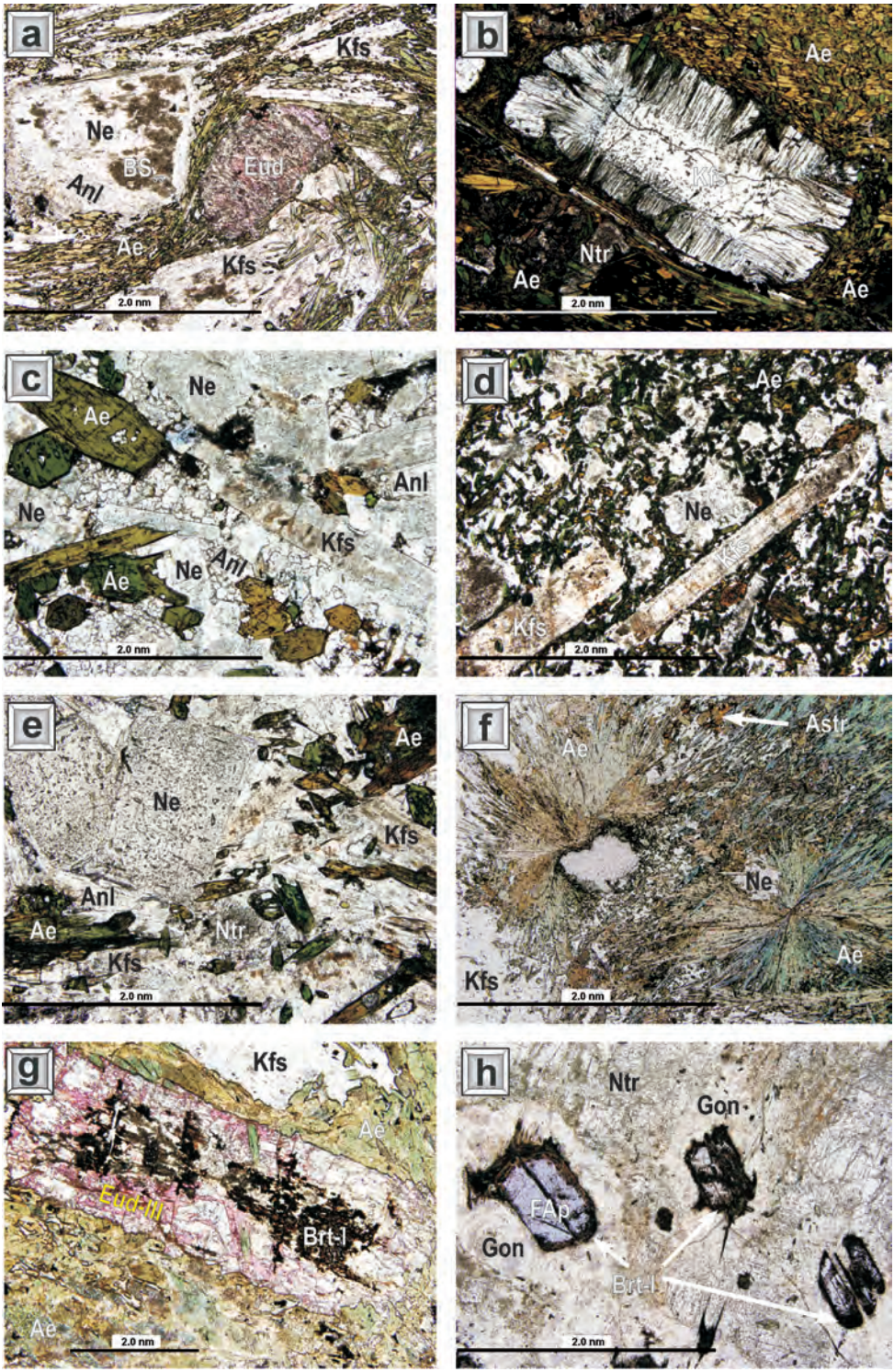
a
Kfs
Ne
BS
Eud
Anl
Ae
Kfs
2.0 nm
b
Ae
Kfs
Ntr
Ae
Ae
2.0 nm
c
Ne
Ae
Anl
Ne
Kfs
Ne
Anl
Ae
2.0 nm
d
Ae
Ne
Kfs
Kfs
2.0 nm
e
Ae
Ne
Kfs
Anl
Ae
Ntr
Kfs
2.0 nm
f
Astr
Ae
Ne
Ae
Kfs
2.0 nm
g
Kfs
Ae
Eud-III
Brt-I
Ae
2.0 nm
h
Ntr
Gon
FAp
Gon
Brt-I
2.0 nm

At the termination of the 'hyperagpaitic' stage, alkalinity decreased as indicated by re-current generations of 'agpaitic' minerals, including the latest generation of hydrothermal eudialyte-III (Mitchell and Liferovich, 2006). Associated with these minerals is a *LREE*-rich variety of Sr-apatite (referred to hereafter as SrAp-*LREE*). Commonly, aggregates of SrAp-*LREE* mantle Sr-apatite (Fig. 3*d*) or form intergrowths with previous generations of apatite-group minerals (Fig. 3*g*). In turn, SrAp-*LREE* is altered at contacts with later natrolite and an unidentified Ca-Na zeolite (gonnardite?). Following extensive development of natrolite at the expense of aluminosilicates in lujavrite, unaltered SrAp-*LREE* has not been preserved and is replaced by late britholite-II and *LREE*-fluorocarbonates.

At the stage of low-temperature replacement of analcime and other aluminosilicates by natrolite, rare Sr-Na-*LREE*-rich varieties of apatite approaching the stoichiometry of belovite-(Ce) and deloneite-(Ce) (see below) crystallized at the expense of FAp-Sr, SrAp and SrAp-*LREE* (Fig. 3*d*). Similar Sr-Na-*LREE* apatite-group minerals occur as discrete grains enclosed by natrolite (Fig. 3*h*). At the lowest temperatures of alteration, these minerals were also subjected to alteration and replacement by diverse *LREE*-rich minerals.

The last of the apatite-group minerals to form was fine-grained, late-stage britholite (Brt-II; Fig. 3*b*,*d*,*h*) in association with natrolite and 'miaskitic' phases such as pyrochlore, strontianite, biotite, fluorite, *LREE*-fluorocarbonates, monazite-(Ce), and late fibrous silica (an unidentified polymorph). The late-stage britholite appears as alteration patches or reaction-induced rims, which typically do not exceed 1–5 μm in thickness, or as microscopic grains in decomposed *LREE*-rich minerals.

Together with apatite and britholite, low-temperature fine-grained aggregates of complex mineralogy contain a number of unidentified phospho-arsenates, arsenates and *LREE* silicates, which might belong to the apatite group. Unfortunately, their small size and intergrowths with other minerals precludes identification (Mitchell and Liferovich, 2004).

Analytical methods

All mineral compositions were determined by Quantitative Energy-Dispersion X-ray Spectrometry (EDXA) using a JEOL JSM-5900 Scanning Electron Microscope (SEM) equipped with a Link ISIS 300 analytical system incorporating a Super ATW Element Detector (133 eV FwHm Mn*K*). Raw EDS spectra were acquired for 130 s (live time) with an accelerating voltage of 20 kV, and beam current of 0.475 nA on a Ni standard. Spectra were processed with the LINK ISIS-SEMQUANT quantitative software package with full ZAF corrections. The following well characterized mineral and synthetic standards were used: benitoite (Ba), fluorapatite BM 1926-665 (P, F, Ca), corundum (Al), jadeite BM 1913-451 (Na), ilmenite (Fe), Mn-fayalite (Mn), loparite (Ce, La, Pr, Nd), orthoclase (K), NaCl (Cl), $SrTiO_3$ (Sr), YF_3 (Y), and pyroxene DJ-35 (Si). Thorium was observed in britholite in amounts ranging from trace to ~2 wt.% ThO_2, but was not quantified because of the lack of a suitable standard. Although anisotropic diffusion of halogens during electron-microprobe analysis has been demonstrated to affect the X-ray intensities of these elements (Stormer *et al.*,

FIG. 2 (*facing page*). Characteristic textural and mineralogical features of nepheline syenites, Pilansberg peralkaline Complex, South Africa. All photomicrographs were taken in plane-polarized light. (*a*) Lujavrite with microphenocrysts of eudialyte, alkali feldspar and nepheline embedded into a flow-aligned and foliated aggregate of acicular aegirine. Note the extensive alteration of nepheline (preserved only in the core of the crystal) with replacement by fine-grained aggregates of stronalsite and analcime (rim). (*b*) An alkali feldspar phenocryst in melanolujavrite, consisting of ordered microcline with aegirine microlites. (*c*) Inequigranular lujavrite. (*d*) Porphyritic lujavrite. (*e*) Ledig foyaite. (*f*) White foyaite. (*g*) A complex eudialyte microphenocryst in lujavrite. The core consists of a mixture of early eudialyte-I replaced by a mixture of britholite-(Ce), zircon, strontiopyrochlore and allanite-(Ce) followed by a deuteric Na-Zr-Si phase; hydrothermal eudialyte-III forms the strongly-pleochroic margins of the aggregate. (*h*) Partially-altered and replaced crystals of fluorapatite-I in white foyaite which are mantled by Ca-Na zeolite (gonnardite?) at the contact with natrolite (similar to Fig. 3*d*). Ae: aegirine, Anl: analcime, Astr: astrophyllite, Brt: britholite (in aggregate with other phases), BS_{ss}: banalsite-stronalsite, clinopyroxene, Eud: eudialyte, Gon: a Ca-Na zeolite (gonnardite?), KFsp: alkali feldspar, SrNa*LREE*: Sr-Na-*LREE* apatite, Ne: nepheline, Ntr: natrolite, NZS: an unidentified deuteric Na-Zr-Si phase.

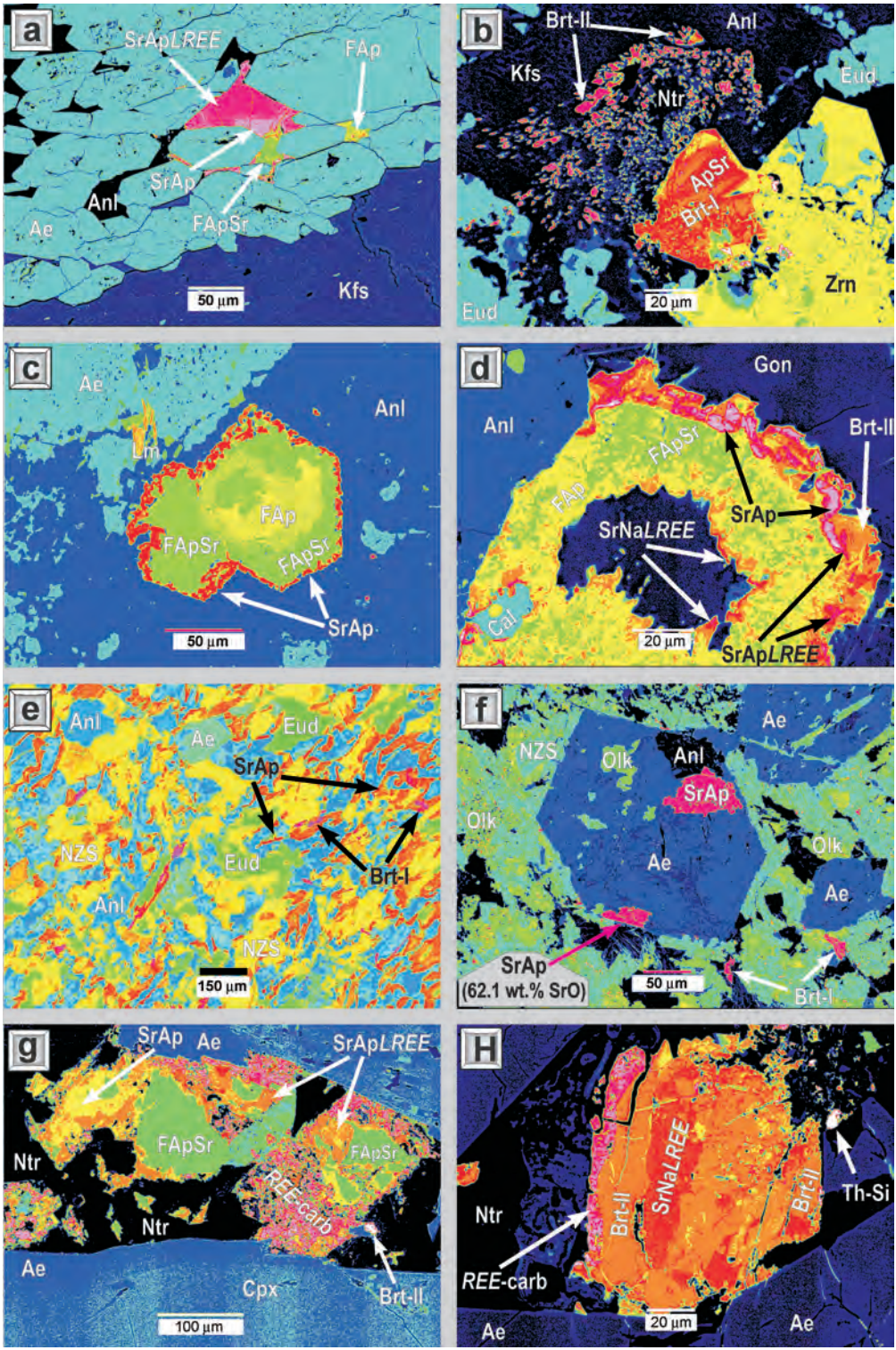
a
SrApLREE
FAp
SrAp
Anl
Ae
FApSr
50 µm
Kfs
b
Brt-II
Anl
Kfs
Ntr
Eud
ApSr
Brt-I
Zrn
Eud
20 µm
c
Ae
Anl
Lm
FAp
FApSr
FApSr
50 µm
SrAp
d
Gon
Anl
Brt-II
FApSr
FAp
SrAp
SrNaLREE
Cal
20 µm
SrApLREE
e
Anl
Ae
Eud
SrAp
NZS
Eud
Brt-I
Anl
NZS
150 µm
f
Ae
NZS
Olk
Anl
SrAp
Olk
Olk
Ae
Ae
SrAp
(62.1 wt.% SrO)
50 µm
Brt-I
g
SrAp
Ae
SrApLREE
FApSr
FApSr
Ntr
REE-carb
Ntr
Ae
Cpx
Brt-II
100 µm
H
Brt-II
SrNaLREE
Brt-II
Th-Si
Ntr
REE-carb
Ae
20 µm
Ae

1993), this effect is considered as insignificant in our data as we employed low-beam currents, and used a standard the surface of which was not normal to the direction of preferential diffusion (Chakhmouradian *et al.*, 2002). A multi-element standard for *LREE* was used as with EDS spectrum-stripping techniques; this provides more accurate data than using single-*LREE* standards. However, peak profiles used for the analytical lines were established using individual *LREE* fluoride standards. The accuracy of the EDXA technique employed here has been confirmed by WDS-EMPA (wavelength-dispersion electron microprobe analysis) using an automated CAMECA SX-50 microprobe (University of Manitoba, Purdue University) following methods described by Mitchell and Vladykin (1993) and Chakhmouradian and Mitchell (2002). The accuracy of the analysis of individual *LREE* was monitored by analysing WDS-analysed belovite-(La) and loparite-(Ce). The reliability of the Na analyses was checked using the approach described by Mitchell and Liferovich (2004, 2005). Additionally, the accuracy of the analyses was cross-checked by WDS-EMPA of complex astrophyllite-kupletskite solid-solution series minerals from Pilansberg lujavrite. Quantitative data obtained for these minerals by WDS are in good agreement with those obtained by our EDXA method. Our conclusions regarding apatite-group minerals are based on 288 original compositions.

Compositional variations of apatite-group minerals

At Pilansberg, apatite-group minerals are systematically enriched in Sr and F. Less commonly, they are enriched in Na, *LREE* and Si. The composition of britholite is essentially controlled by the composition of precursor phases that were subjected to alteration and replacement. In common with apatite from diverse alkaline parageneses (Chakhmouradian and Mitchell 1999, 2002; Chakhmouradian *et al.*, 2002, 2005), the compositional variation of these minerals can be considered in terms of combinations of the following simplified substitutional schemes involving the four end-member compositions: $Ca_5(PO_4)_3X$, $Sr_5(PO_4)_3X$, $Na_{2.5}LREE_{2.5}(PO_4)_3X$, and $Ca_2LREE_3(TO_4)_3X$, where T = P, Si and X is predominantly F:

(1) Apatite–Sr-apatite join:

$Ca^{2+} \rightleftharpoons Sr^{2+}$ (Pushcharovsky *et al.*, 1987; Rakovan and Huges, 2000; Chakhmouradian *et al.*, 2002);

(2) Apatite–belovite join:

$5Ca^{2+} \rightleftharpoons 3Sr^{2+} + Na^{+} + LREE^{3+}$ (Nadezhina *et al.*, 1987);

(3) Apatite–deloneite join:

$2Ca^{2+} \rightleftharpoons Na^{+} + LREE^{3+}$ (Khomyakov *et al.*, 1996);

(4) Apatite–britholite:

$Ca^{2+} + P^{5+} \rightleftharpoons Si^{4+} + LREE^{3+}$ (Pan and Fleet, 2002).

FIG. 3 (*facing page*). False-colour back-scattered electron images of apatite-group minerals. (*a*) Interstitial apatite-group minerals in a flow-aligned aegirine aggregate in lujavrite. Note that later generations occur both as independent interstitial grains and rims around early fluorapatite grains. (*b*) Complex aggregate formed by alteration and replacement of britholite-I by late Sr-apatite and *REE*-carbonate(s) in contact with analcime and britholite-II enclosed by natrolite, which replaces analcime. (*c*) A complex apatite aggregate with a core composed of strongly-corroded fluorapatite (FAp), cemented and entrapped by strontian fluorapatite (FAp-Sr), finally mantled by Sr-apatite (SrAp). (*d*) Complex alteration of fluorapatite (yellow) and strontian fluorapatite (green) and their successive replacement by Sr-apatite (pink), *LREE*-rich Sr-apatite (red), britholite-II (orange), and late Na-Sr-*LREE* apatite. (*e*) Fine-grained Sr-apatite and britholite-I formed by alteration of Sr-rich eudialyte. (*f*) Sr-apatite (red) forming complete pseudomorphs after strontian fluorapatite enclosed by prismatic aegirine-augite. (*g*) Complex alteration of strontian fluorapatite (green) in white foyaite. (h) Textural relationships between strontian fluorapatite (red), britholite-I (orange), and britholite-II (pink).

Generations are given in Roman numerals; Ae-Aug: aegirine-augite (clinopyroxene-I), FApSr: strontian apatite, Anl: analcime, Brt: britholite, Cal: calcite, Eud: eudialyte, FAp: fluorapatite, Kfs: potassic feldspar, Lm: lamprophyllite-group minerals, Ne: nepheline, NZS: an unspecified deuteric Na-Zr-Si phase, Olk: olekminskite, *REE*-carb: rare earth carbonates (ancylite, synchysite or bastnäsite), SrAp: Sr-apatite, SrAp*LREE*: *LREE*-rich Sr-apatite, SrNa*LREE*: Sr-Na-*LREE*-rich apatite, Sod: sodalite, Th-Si: an unidentified deuteric silicate of Th (huttonite?), Zrn: zircon.

Fluorapatite

Orthomagmatic fluorapatite (FAp) occurring as relict cores in later-forming apatite group minerals (Fig. 2*h*, 3*c*) or grains in aegirine interstices (Fig. 3*a*), has an atomic ratio between the large cations and small tetrahedrally-coordinated cations ('*A*:*T* ratio') close to the 'ideal' stoichiometric value of 1.67 (Table 1, comp. 1–4). The apatites contain 0.72–0.93 a.p.f.u. F, up to 1 wt.% Na_2O and 4.2 wt.% SrO (Fig. 4). In sodalite-rich white foyaite, less altered crystals of fluorapatite contain up to 5.6-6.3 wt.% $LREE_2O_3$ and 2.4 wt.% SiO_2 ($\geqslant$0.20 and ~0.21 a.p.f.u. *LREE* and Si, respectively). Typically, the margins of the crystals are slightly enriched in *LREE* and Si relative to the cores, whereas Sr-enriched areas appear as irregular domains within the larger crystals. The *LREE* content does not correlate with Sr and/or Na, but does with Si (Figs 5, 6), thus demonstrating the presence of the 'britholite substitution scheme'. A similar compositional trend has been described for orthomagmatic fluorapatite in nepheline syenite, including lujavrite, from the Ilímaussaq sodic peralkaline complex (Fig. 5; Rønsbo, 1989). This trend culminates in the crystallization of the earliest generation of britholite (Brt-I), which followed/replaced FAp (Fig. 2*h*) during the earliest 'miaskitic' post-magmatic stage. The *LREE* content is variable and in some instances La-enriched compositions are found (Table 1, comp. 3).

Strontian fluorapatite

Strontian fluorapatite (FAp-Sr) exhibits intergrain, but not intragrain compositional variation (Fig. 3*c*,*g*) reflecting, principally, simple isovalent

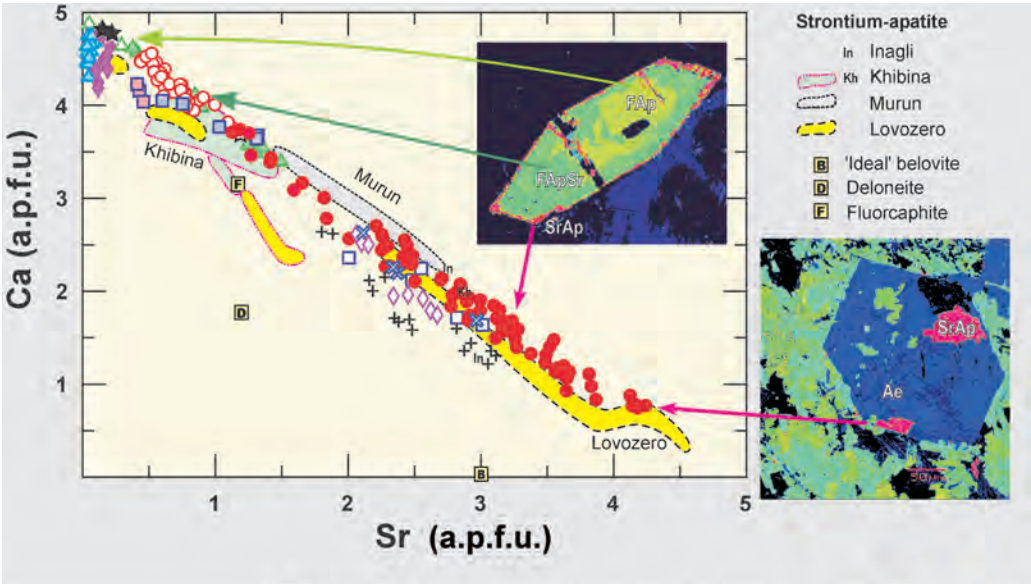

	Paragenesis (see Fig. 7 for details)	Lujavrite Melanolujavrite	Inequigranular and porphyritic lujavrite	White foyaite	Ledig foyaite
Fluorapatite	Orthomagmatic	△	△	△	♦
Fluorapatite in pegmatoids			★	□	
Strontian fluorapatite	Moderate alkalinity	▲	○	☆	□
Strontium-apatite	Maximum alkalinity	□	●		
Strontium-apatite, *REE*-rich			+	✖	◊

FIG. 4. Variation of Ca *vs.* Sr (mol.%) in apatite-group minerals. Also shown are compositional data for apatite-group minerals from alkaline rocks of the Inagli, Khibina, Lovozero and Murun (after Efimov *et al.*, 1962; Rønsbo, 1989; Pekov *et al.*, 1995; Khomyakov *et al.*, 1996, 1997; Chakhmouradian *et al.*, 2002).

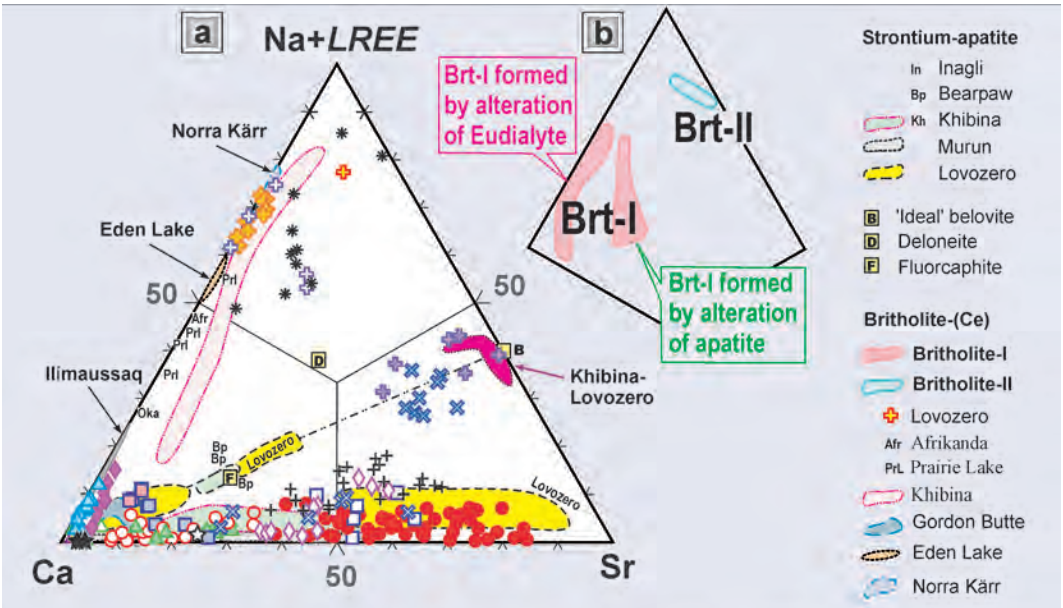

	Paragenesis (see Fig. 7 for details)	Lujavrite Melanolujavrite	Inequigranular and porphyritic lujavrite	White foyaite	Ledig foyaite
Fluorapatite	Orthomagmatic	△	▲	▲	♦
Fluorapatite in pegmatoids	Orthomagmatic		★	■	
Strontian fluorapatite	Moderate alkalinity	▲	○	☆	□
Strontium-apatite	Maximum alkalinity	□	●		
Strontium-apatite, *REE*-rich	Maximum alkalinity		+	✖	◇
Sr-Na-*LREE*-rich apatite	Decreasing alkalinity		✤	✖	
Britholite-(*REE*), Brt-I and Brt-II	Moderate alkalinity / Decreasing alkalinity	✤	*		✤

FIG. 5. (*a*) Variation in apatite-group minerals in the pseudoternary system $Ca(PO_4)_3X$ – $Sr(PO_4)_3X$ – $(Na,LREE)(TO_4)_3X$. Also shown are compositional data for apatite-group minerals from Norra Kärr and Prairie Lake (our data), Khibina (incl. our data), Afrikanda, Bearpaw Mountains, Gordon Butte, Eden Lake, Ilímaussaq, Inagli, Lovozero and Murun (after Efimov *et al.*, 1962; Rønsbo, 1989; Pekov *et al.*, 1995; Khomyakov *et al.*, 1996, 1997; Arden and Halden, 1999; Chakhmouradian and Mitchell, 1999; Chakhmouradian *et al.*, 2002; Zaitsev and Chakhmouradian, 2002; Chakhmouradian *et al.*, 2005). (*b*) Composition variations of Pilansberg britholite depending on generation and on precursor phase subjected to alteration and replacement (for Brt-I).

Sr-for-Ca substitutions (Fig. 4). This diadochy does not affect the *A:T* ratio, which remains close to the theoretical value of 1.67 (Table 1, comp. 5–9). The material with the greater concentrations of Sr is restricted to extensively altered rocks, demonstrating clearly that the more-strontian compositions are the more evolved. Sr contents range from 8.2 wt.% SrO to ~27 wt.% SrO (0.41–1.50 a.p.f.u. Sr; Table 1). The mineral contains up to ~3 wt.% $LREE_2O_3$, 0.5 wt.% Na_2O, 0.6 wt.% SiO_2, and 0.5 wt.% FeO. The *X* site in FAp-Sr is dominated by F (0.78–1.0 a.p.f.u. F), which is present in greater amounts than in the orthomagmatic FAp (cf. Table 1, comp. 1–4 *vs.* 5–9).

Sr-apatite

Typically, the abundance of Sr increases from cores to margins of SrAp grains and correlates positively with the extent of subsolidus alteration of the host syenite. In common with earlier

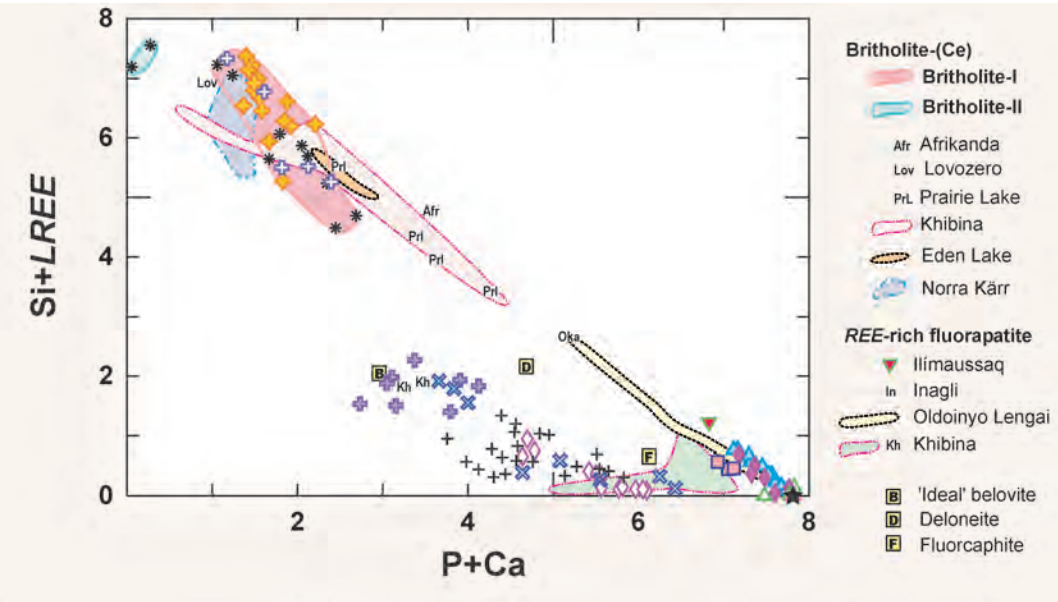

	Paragenesis (see Fig. 7 for details)	Lujavrite Melanolujavrite	Inequigranular and porphyritic lujavrite	White foyaite	Ledig foyaite
Fluorapatite	Orthomagmatic	△	△	△	♦
Fluorapatite in pegmatoids	Orthomagmatic		★	□	
Strontium-apatite, *REE*-rich	Maximum alkalinity		+	⊠	◇
Sr-Na-*LREE*-rich apatite	Decreasing alkalinity		✤	⊠	
Britholite-(*REE*), Brt-I and Brt-II	Moderate alkalinity / Decreasing alkalinity	◆	✱		✤

FIG. 6. Variation of P+Ca *vs.* Si+*LREE* (atoms per formula unit) in apatite-group minerals. Also shown are compositional data for apatite-group minerals from Norra Kärr and Prairie Lake (our data), Khibina (incl. our data), Afrikanda, Eden Lake, Ilímaussaq, Inagli, Lovozero and Oldoinyo Lengai (after Efimov *et al.*, 1962; Rønsbo, 1989; Pekov *et al*., 1995; Khomyakov *et al*., 1996, 1997; Arden and Halden, 1999; Chakhmouradian and Mitchell, 1999; Chakhmouradian *et al*., 2002; Mitchell and Belton, 2004; Zaitsev and Chakhmouradian, 2002; Chakhmouradian *et al*., 2005).

varieties of fluorapatite, unaltered SrAp commonly has a stoichiometric composition with an *A:T* ratio of ~1.66–1.69 (Table 2, comp. 1–9). In common with holotype Sr-apatite from Inagli (Efimov *et al.*, 1962) and Sr-apatite from Khibina and Lovozero (Khomyakov, 1990, 1995; Pekov, 2001; Chakhmouradian *et al.*, 2002), the *X* site in Sr-apatite from Pilansberg is dominated by F (0.74–1 a.p.f.u. F). Following the existing nomenclature of the apatite group, this species should be classified as an 'F-dominant analogue' of Sr-apatite; the latter is currently considered to be OH-dominant, $(Sr,Ca)_5(PO_4)_3(OH,F)$ (Mandarino, 1999). However, in this work, the term Sr-apatite (SrAp) is used for this F-dominant species, which is similar to the F-dominant holotype Sr-apatite from Inagli (Efimov *et al.*, 1962), and examples from Khibina and Lovozero (Khomyakov, 1995; Chakhmouradian *et al.*, 2002). Our data provide further support for re-definition of the curious 'theoretical' Sr-apatite in which the *X*-site is considered to be filled by hydroxyl ions (e.g. Chakhmouradian *et al.*, 2002).

The range of SrO variation between cores and the most strontian margins is as great as 22–25 wt.% SrO. The relatively Sr-poor areas contain only 1.13 a.p.f.u. Sr, i.e. are not Sr-apatite *sensu lato*. Such material might be partially-pseudomorphed relics of earlier FAp-Sr corroded and mantled by Sr-apatite. The majority of

TABLE 1. Representative compositions of fluorapatite and strontian fluorapatite.

	Fluorapatite				Strontian fluorapatite				
	1	2	3	4	5	6	7	8	9
Na_2O	0.32	0.73	1.00	–	–	0.10	0.22	0.18	0.46
CaO	54.05	51.17	47.64	50.25	49.42	42.69	36.05	33.15	32.87
SrO	1.02	4.20	3.11	0.81	8.18	16.26	23.99	22.93	26.77
BaO	–	–	–	–	–	–	–	–	–
MnO	–	–	–	–	–	–	–	–	0.23
FeO_t	–	–	–	0.28	0.16	0.46	–	0.53	0.10
Ce_2O_3	1.56	0.79	2.60	4.81	–	0.12	–	1.07	–
La_2O_3	0.74	–	2.69	1.47	–	–	–	1.85	0.26
Nd_2O_3	–	–	0.31	–	–	–	–	–	0.34
P_2O_5	41.42	41.38	40.18	37.18	41.13	39.22	37.20	35.74	35.83
SiO_2	0.00	0.54	0.18	2.44	0.00	0.00	0.39	0.54	0.64
F	3.02	2.84	2.59	3.34	2.86	3.54	2.90	3.27	3.30
O=F	−1.27	−1.20	−1.09	−1.41	−1.20	−1.49	−1.22	−1.38	−1.39
Total	100.86	100.45	99.21	99.17	100.55	100.90	99.53	97.88	99.41
Structural formulae calculated on the basis of 8 cations:									
Na	0.052	0.120	0.170	–	–	0.017	0.040	0.034	0.086
Ca	4.875	4.639	4.485	4.745	4.572	4.112	3.642	3.487	3.390
Sr	0.050	0.206	0.158	0.041	0.410	0.848	1.312	1.306	1.494
Ba	–	–	–	–	–	–	–	–	–
Mn	–	–	–	–	–	–	–	–	0.019
Fe_t	–	–	–	0.021	0.012	0.035	–	0.044	0.008
La	0.023	–	0.087	0.048	–	–	–	0.067	0.009
Ce	0.048	0.024	0.084	0.155	–	0.004	–	0.038	–
Nd	–	–	0.010	–	–	–	–	–	0.012
P	2.952	2.965	2.989	2.774	3.007	2.985	2.969	2.971	2.920
Si	–	0.046	0.016	0.215	–	–	0.037	0.053	0.062
LREE	0.071	0.024	0.181	0.203	–	0.004	–	0.105	0.021
F	0.804	0.760	0.720	0.931	0.781	1.006	0.865	1.015	1.005
A/T	1.71	1.66	1.66	1.68	1.66	1.68	1.66	1.65	1.68
Σ_A	5.05	4.99	5.00	5.01	4.99	5.01	4.99	4.98	5.02
Σ_T	2.95	3.01	3.01	2.99	3.01	2.99	3.01	3.02	2.98

– not detected; *LREE* light rare earth elements
1, 5, 6 and 8 in lujavrite; 2 in porphyritic lujavrite; 3 and 7 in Ledig foyaite; 4 in pegmatoid white foyaite; 9 in massive white foyaite

analysed SrAp grains contain $\geqslant 2$ a.p.f.u. Sr, i.e. significantly more Sr than present in precursor FAp-Sr (Fig. 4). In lujavrite subjected to the most extensive autometasomatic alteration, as indicated by the total alteration and replacement of primary nepheline and potassic feldspar, ApSr contains up to 62.1 wt.% SrO (4.24 a.p.f.u. Sr; Table 2, comp. 9, Fig. 3*f*). This material is richer in Sr than that of the holotype Sr-apatite from Inagli, and other examples from hydrothermally-altered Khibina hyperagpaitic pegmatites (Efimov, 1962; Khomyakov, 1995; Fig. 4). Assuming complete occupation of all three ^{VII}Ca(2) positions by Sr according to the site preference scheme described by Rakovan and Hughes (2000), the remaining Sr in the most Sr-rich compositions is sufficient to occupy ~57−63% of sites available at the two ^{IX}Ca(1) positions. Thus, even if retaining an ordered $P6_3$ structure typical of $^{IX}Ca_2{}^{VII}Sr_3(PO_4)_3X$ Sr-apatite, this phase contains enough Sr to dominate all of the large-cation sites.

SrAp contains up to 0.7 wt.% Na_2O, 4.7 wt.% $LREE_2O_3$, 0.8 wt.% FeO, and 1.4 wt.% SiO_2. Ba and Mn are commonly below the detection limit. Na correlates antipathetically with Sr, whereas *LREE* and Si do not correlate with Sr (Table 2, comp. 1−9), thus suggesting that the Na- and *LREE*-bearing varieties of SrAp do not evolve

TABLE 2. Representative compositions of Sr-apatite.

	Sr-apatite									*LREE*-rich Sr-apatite					
	1	2	3	4	5	6	7	8	9	10*	11	12	13	14	15
Na_2O	0.55	0.40	0.26	0.44	0.74	0.44	0.20	0.13	–	0.80	1.13	0.34	0.71	0.55	0.65
CaO	36.88	29.91	28.71	22.15	20.04	13.13	10.74	6.16	6.10	19.96	11.72	8.67	15.89	19.25	18.24
SrO	20.71	28.85	32.22	37.41	37.73	48.98	52.56	61.66	62.06	37.07	43.96	54.70	41.71	38.02	35.65
BaO	–	–	0.25	0.21	–	–	–	–	–	–	1.14	–	–	0.18	–
FeO_t	0.35	0.37	–	0.75	0.16	–	–	–	–	–	–	–	–	–	–
Ce_2O_3	0.75	1.35	0.43	1.33	2.70	1.77	2.51	0.95	0.39	3.85	3.46	3.05	3.68	3.88	5.63
La_2O_3	–	0.81	0.93	1.07	1.95	2.22	1.08	–	–	2.87	4.17	2.25	2.95	2.84	2.75
Pr_2O_3	–	–	–	–	0.24	0.14	–	–	–	–	–	–	–	0.27	0.46
Nd_2O_3	–	0.45	0.20	–	1.02	0.16	–	–	–	–	–	–	0.45	0.46	2.43
Sm_2O_3	–	–	–	–	0.43	–	–	–	–	–	–	–	–	–	0.49
P_2O_5	37.81	34.98	34.77	31.75	32.30	31.76	29.82	29.21	29.55	32.20	30.48	29.66	30.93	31.70	29.26
SiO_2	–	0.51	0.63	1.42	1.07	–	0.93	0.86	0.22	1.10	0.42	0.81	1.21	1.07	2.10
F	2.98	2.95	2.72	3.00	2.20	2.13	2.38	2.72	2.70	2.53	2.75	2.78	2.42	1.62	2.35
O=F	−1.25	−1.24	−1.15	−1.26	−0.93	−0.90	−1.00	−1.15	−1.14	−1.07	−1.16	−1.17	−1.02	−0.68	−0.99
Total	98.78	99.34	99.97	98.27	99.65	99.83	99.22	100.54	99.88	99.52	98.07	101.09	98.93	99.16	99.02
Structural formulae calculated on the basis of 8 cations:															
Na	0.100	0.077	0.050	0.090	0.152	0.095	0.044	0.029	–	0.165	0.251	0.076	0.152	0.115	0.139
Ca	3.712	3.167	3.050	2.493	2.271	1.568	1.318	0.770	0.770	2.269	1.441	1.069	1.877	2.216	2.153
Sr	1.128	1.654	1.852	2.278	2.314	3.165	3.490	4.173	4.240	2.280	2.925	3.649	2.666	2.369	2.277
Ba	–	–	0.010	0.009	–	–	–	–	–	–	0.051	–	–	0.008	–
Fe_t	0.027	0.031	–	0.066	0.014	–	–	–	–	–	–	–	–	–	–
La	–	0.030	0.034	0.041	0.076	0.091	0.046	–	–	0.112	0.176	0.095	0.120	0.113	0.112
Ce	0.026	0.049	0.016	0.051	0.105	0.072	0.105	0.041	0.017	0.150	0.145	0.128	0.149	0.153	0.227
Pr	–	–	–	–	0.009	0.006	–	–	–	–	–	–	–	0.011	0.018
Nd	–	0.016	0.007	–	0.039	0.006	–	–	–	–	–	–	0.018	0.018	0.096
Sm	–	–	–	–	0.016	–	–	–	–	–	–	–	–	–	0.019
P	3.007	2.927	2.919	2.823	2.892	2.996	2.891	2.886	2.947	2.892	2.961	2.889	2.886	2.884	2.729
Si	-	0.050	0.062	0.149	0.113	–	0.106	0.100	0.026	0.117	0.048	0.093	0.133	0.115	0.231
LREE	0.026	0.094	0.057	0.093	0.244	0.176	0.151	0.041	0.017	0.262	0.322	0.224	0.286	0.293	0.471
F	0.885	0.922	0.853	0.997	0.736	0.751	0.862	1.004	1.006	0.849	0.998	1.012	0.844	0.551	0.819
A/T	1.66	1.69	1.68	1.69	1.66	1.67	1.67	1.68	1.69	1.60	1.66	1.68	1.65	1.67	1.70
Σ_A	4.99	5.02	5.02	5.03	5.00	5.00	5.00	5.01	5.03	4.99	4.99	5.02	4.98	5.00	5.04
Σ_T	3.01	2.98	2.98	2.97	3.00	3.00	3.00	2.99	2.97	3.01	3.01	2.98	3.02	3.00	2.96

– not detected; *LREE* light rare earth elements; * includes 0.21 wt.% ZnO

1, 4, 13 and 15 in inequigranular lujavrite; 2 and 5 in lujavrite; 3, 6, 7, 8, 9 and in 12 porphyritic lujavrite; 10, 11 and 14 in Ledig foyaite

towards belovite (or deloneite and fluorcaphite), but form an extensive solid solution along the 'apatite–Sr-apatite' join (Figs 4, 5).

LREE-rich Sr-apatite

The next generation of apatite, *LREE*-rich Sr-apatite (SrAp-*LREE*), formed at the termination of the maximum alkalinity stage. It commonly mantles aggregates of SrAp (Fig. 3*d*), or in rare cases fills interstices in aegirine aggregates (Fig. 3*a*). The mineral is F-rich (0.55–1 a.p.f.u. F) and is distinguished from the previous SrAp generation by a lesser Sr content and notable enrichment in *LREE* (Figs 5, 6), with the total $LREE_2O_3$ ranging up to 14.2 wt.%. The Ce/La ratio is highly variable from sample to sample. In zoned aggregates of SrAp-*LREE*, margins of crystals are less strontian than cores and the observed difference in SrO content can be as great as 12 wt.%. La-dominant compositions are found in Ledig foyaite (Table 2, comp. 11). In most instances, the mineral contains small but detectable amounts of Na (0.6–1.5 wt.% Na_2O) and Si (0.8–2.1 wt.% SiO_2). Fe and Mn are not detectable and Ba is rarely present (Table 2). In the 'Ca-Sr-(Na+*LREE*)' ternary diagram (Fig. 5), the compositional field of SrAp-*LREE* shows a poorly-defined trend subparallel to the 'apatite–belovite' join. In the binary 'P+Ca *vs*. Si+*LREE*' diagram (britholite scheme: Fig. 6), compositions of SrAp-*LREE* also define a diffuse trend towards the composition of belovite rather than that of britholite. As all SrAp-*LREE* compositions considered here have no significant analytical deficiencies and/or conspicuous deviations from theoretical stoichiometry (Table 2), these trends are considered not to be produced by the subsolidus leaching of large cations from A_i sites, and reflect compositional variations of the mineral-forming fluids.

Sr-Na-LREE apatite

The most variable compositions are observed for the apatite-group minerals formed contemporaneously with the latest (late-postmagmatic) generation of 'agpaitic' minerals such as eudialyte-III (Mitchell and Liferovich, 2006) and Mn-rich minerals of the lamprophyllite group, formed during the stage of conversion of analcime to natrolite. The Sr-Na-*LREE*-rich apatite was formed by interaction between previously-formed phosphates and a fluid phase during decreasing alkalinity. In some instances, alteration of the earlier-formed phosphates terminated at an incipient stage resulting in slightly-modified compositions of SrAp-*LREE*, showing an increase in Na_2O contents (1.5–2 *vs*. 0.3–1.1 wt.%; cf. Table 3 comp. 1 and Table 2 comp. 10–15). Further alteration and replacement of FAp-Sr, ApSr and SrAp-*LREE* produced Sr-Na-*LREE*-rich apatite as reaction-induced discontinuous rims 5–30 μm in thick (Fig. 3*d*), or complete pseudomorphs (Fig. 3*h*). The pseudomorphs, where unaltered, typically do not exhibit compositional zoning. In the 'Ca-Sr-(Na+*LREE*)' ternary diagram (Fig. 5), compositions of Sr-Na-*LREE*-rich phosphates plot as a diffuse field at the belovite end of the 'apatite–belovite' join (Ca_5–Na*LREE*Sr_3). More variable and less strontian compositions with higher Na-*LREE* abundances are found in the late phosphates from inequigranular and porphyritic lujavrite. Their counterparts from white foyaite are usually more strontian (Fig. 5, Table 3) and some of these minerals plot close to the composition field of belovite-(Ce) (Pekov *et al*., 1995, 1996). Compositions transitional to deloneite-(Ce), $NaCa_2SrCe(PO_4)_3F$, are also found (Figs 5, 6). The Sr-Na-*LREE* apatite-group minerals contain ~1 a.p.f.u. Ca and ~1±0.2 a.p.f.u. *LREE*. Thus, their compositional variation is due principally to variations in their Na and Sr contents (Table 3). In common with belovite and deloneite, Sr-Na-*LREE* apatite is F-rich, with $\geqslant$0.86 a.p.f.u. F. A comparison of compositional ranges for belovite, deloneite and fluorcaphite from Khibina and Lovozero with those of Sr-Na-*LREE* apatite from Pilansberg is given in Table 3 and Figs 4, 5 and 6. The abundances of Sr and Na in Sr-Na-*LREE* apatite from Pilansberg is close to, but slightly-lower than those in belovite, whereas the abundance of Ca is significantly greater than that of belovite but less than that of deloneite. The Sr-Na-*LREE* apatite also differs from fluorcaphite, initially described as 'Na-Sr-Ce apatite' from Khibina (Khomyakov *et al.*, 1996), this being less strontian (1.17 a.p.f.u. Sr), more calcian (3.16 a.p.f.u. Ca), and poor in *LREE* (~0.33 a.p.f.u. *LREE*; Table 3). Given that compositionally-induced phase transitions from the apatite archetype ($P6_3/m$) are known for Sr-apatite (*sp. gr.* $P6_3$), fluorcaphite ($P6_3$), belovite ($P\bar{3}$) and deloneite ($P3$) occur as a result of ordering of large-size cations at the *A* sites and splitting of crystallographic positions (Chakhmouradian *et*

TABLE 3. Representative compositions of Sr-Na-*LREE* apatite-group minerals replacing strontian apatite and Sr-apatite in postmagmatic assemblages with comparison to compositional ranges of belovite-(Ce), belovite-(La), deloneite-(Ce) and fluorcaphite.

	1	2	3	4	5	6	7	8	Belovite[1,2]	Deloneite-(Ce)[3]	Fluorcaphite[4]
Na_2O	1.81	2.58	2.57	2.77	3.76	3.88	5.44	3.96	3.59–4.9	4.4	1.3–2.4
CaO	15.19	9.58	7.85	10.38	8.19	7.62	2.37	3.42	0.2–3.8	14.8	20.6–32.7
SrO	38.08	36.44	36.23	31.57	30.55	34.72	35.66	38.78	36.1–44.2	18.2	17.7–26.8
BaO	–	–	0.90	–	0.60	–	0.87	0.60			
FeO_t	–	–	0.26	0.32	0.42	–	–	–			
Ce_2O_3	5.36	8.18	10.68	10.35	10.43	10.58	9.84	9.92	$LREE_2O_3$	$LREE_2O_3$	$LREE_2O_3$
La_2O_3	2.21	9.88	9.95	9.22	7.42	6.38	6.21	5.05	20.1–22.9	26.6	9.4–15.8
Pr_2O_3	–	–	–	0.45	0.41	1.54	0.98	0.95			
Nd_2O_3	2.68	1.67	–	1.56	2.43	4.19	2.04	1.82			
Sm_2O_3	–	–	–	0.24	0.76	–	–	–			
P_2O_5	30.98	28.82	28.46	29.43	29.36	29.08	26.40	27.83	28.7–31.3	30.7	33.0–36.2
SiO_2	0.87	1.45	1.12	1.88	1.14	1.35	9.32	4.87	0.1–0.48	0.74	0–0.8
F	2.90	2.77	2.41	2.38	2.68	2.76	1.71	1.89	1.7–2.3	2.0	1.7–3.5
O=F	−1.22	−1.17	−1.01	−1.00	−1.13	−1.16	−0.72	−0.80			
Total	98.86	100.20	99.42	99.55	98.07	100.94	100.12	98.29			
Structural formulae calculated on the basis of 8 cations:											
Na	0.386	0.576	0.588	0.615	0.848	0.859	1.160	0.890	0.83–1.12	0.97	0.24–0.49
Ca	1.791	1.182	0.993	1.274	1.020	0.932	0.279	0.425	0.03–0.48	1.77	2.36–3.42
Sr	2.430	2.433	2.480	2.096	2.060	2.298	2.274	2.608	2.62–3.07	1.18	1.0–1.63
Ba	–	–	0.042	–	0.027	–	0.037	0.027			
Fe_t	–	–	0.026	0.031	0.041	–	–	–			
La	0.090	0.420	0.433	0.389	0.318	0.269	0.252	0.216			
Ce	0.216	0.345	0.462	0.434	0.444	0.442	0.396	0.421			
Pr	–	–	–	0.019	0.017	0.064	0.039	0.040			
Nd	0.105	0.069	–	0.064	0.101	0.171	0.080	0.075			
Sm	–	–	–	0.009	0.030	–	–	–			
P	2.886	2.809	2.844	2.853	2.890	2.811	2.458	2.732	2.96–3.11	2.91	2.92–3.0
Si	0.096	0.167	0.132	0.215	0.133	0.154	1.025	0.565	0.01–0.05	0.08	0–0.08
LREE	0.411	0.833	0.895	0.915	0.966	0.946	0.767	0.753	0.88–1.05	1.09	0.33–0.62
F	1.009	1.009	0.900	0.862	0.985	0.997	0.595	0.693	0.62–0.88	0.72	0.65–0.99
A/T	1.68	1.69	1.69	1.61	1.65	1.70	1.30	1.43	1.56–1.67	1.67	1.62–1.69
Σ_A	5.02	5.02	5.02	4.93	4.98	5.03	4.52	4.70	4.87–5.01	5.01	4.95–5.03
Σ_T	2.98	2.98	2.98	3.07	3.02	2.97	3.48	3.30	2.99–3.13	2.99	2.97–3.05

– not detected; 1 sodic variety of Sr-LREE Sr-apatite (SrAp*LREE*); 1, 2, 3 and 6 in white foyaite; 4 in Ledig foyaite; 5 in inequigranular lujavrite; 7 and 8 in porphyritic lujavrite; * includes 0.15 wt.% MnO and 0.89 wt.% Y_2O_3; [1] Belovite-(Ce) (Pekov *et al.* 1995), [2] Belovite-(La) (Pekov *et al.* 1996), [3]Khomyakov *et al.* (1996), [4]Khomyakov *et al.*, (1997), Chakhmouradian *et al.* (2005)

al., 2005 and references therein), the Sr-Na-*LREE* apatite, if ordered, might crystallize in the $P\bar{3}$ or *P*3 space groups. If this were the case, its crystal chemical formula, following Khomyakov *et al.* (1996), might be expressed as $(Na_{2-x}Ca_x)(Ca,Sr)(LREE,Sr)Sr_2(PO_4)_6(F,OH)$ with some compositions evolving to $CaLREESr_3(PO_4)_6F$ (e.g. Table 3, comp. 2,3).

One specific variety of Sr-Na-*LREE* apatite enriched in Si (Table 3, comps. 7-8) occurs as a few grains ranging from 3 to 12 μm in size in a porphyritic lujavrite. This is a product of deuteric alteration of SrAp-*LREE*. In turn, this silicophosphate has been subject to alteration and replacement by later *LREE*-fluorcarbonates, strontianite and britholite-II. This phase contains 0.6−1.03 a.p.f.u. Si and has Ca:Sr:[Na+*LREE*] ratio which plots in the compositional field of belovite (Fig. 5). This observation suggests the existence of a natural solid-solution series between belovite-(Ce) and britholite-(Ce), with a Si-for-P substitutional scheme accompanied by charge-balancing substitutions at the *A* and *X* sites. Calculation of the compositions of this silicophosphate on the basis of 8 cations, demonstrates that it, in common with most of the published belovite compositions, exhibits a deficiency of large and an 'excess' of small tetrahedrally-coordinated cations (Table 3). Such deviations from theoretical stoichiometry might result from the presence of unaccounted actinides, light elements, H_3O^+ or vacancies at the *A*-sites. In contrast, the relatively low abundance of F (0.6−0.7 a.p.f.u. F) permits the presence of higher-charged anions, i.e. O^{2-} and/or CO_3^{2-} anions ('*A*-type substitutions'; Pan and Fleet, 2002).

Britholite

Britholite is a minor phase in Pilansberg nepheline syenite, forming by the breakdown of eudialyte (Figs 2*g*, 3*e*) and other *LREE*-rich minerals, or occurring as reaction rims produced by deuteric alteration of, or as epitaxial overgrowths on precursor apatite (Figs 2*h*, 3*d*,*h*). Britholite also replaces *LREE*-rich minerals such as rinkite, allanite and in some instances pyrochlore and fergusonite. The mineral demonstrates significant compositional variation in terms of its Si/P ratio, proportions of large-size cations, and abundance of F.

The early generation of britholite (Brt-I) was formed during the early-post-magmatic stage before the crystallization of euhedral strontian eudialyte-II (Fig. 2*g*). It is easily distinguished from the later britholite (Brt-II) as this earlier generation preceeded analcime and the hyperagpaitic mineral parageneses, whereas the latter post-dates all of the agpaitic and hyperagpaitic parageneses. The abundance of F in Brt-I ranges from 1.0 to 0.28 a.p.f.u. thus suggesting the presence of several different species, e.g. 'fluor-britholite' akin to material described by Oberti *et al.* (2001), and its F-poor analogues.

Britholite-I is of Ce-dominated composition with low- to undetectable abundances of Y and *REE* heavier than Sm. Britholite-I formed after apatite-group minerals contains 3.5−12.9 wt.% P_2O_5 (Table 4, comp. 6−9). When formed after eudialyte-I and rinkite, Brt-I commonly does not contain detectable P, and hosts concentrations of *LREE* commonly exceeding the 3 a.p.f.u. limit implied by complete substitutions according to an idealized Ca(1) + P $\rightleftharpoons$ Si + *LREE* 'britholite substitution scheme', and ranging from 3.12 to 3.67 a.p.f.u. (Table 4, comp. 1−5). Some of the Brt-I compositions exhibit an excess of *T* cations, which might be an artefact resulting from a deficiency of large cations and normalization of the compositions to 8 cations. The presence of actinides or large-ion light elements (*LILE*) might account for the '*A*-deficient' compositions, whereas the presence of tetrahedrally coordinated carbon and boron (Oberti *et al.*, 2001) might account for the '*A*-excess' varieties of britholite-I. Formation of compositionally-different varieties of Brt-I during the same stage of mineralization implies that the mineral-forming fluids at the early-post-magmatic stage did not reach chemical equilibrium with nepheline syenite. Britholite-I formed by alteration of FAp, is always enriched in P and Sr (4.7−15.7 wt.% SrO). These elements exhibit a strong positive correlation (Table 4, comp. 6−9). The most strontian britholite compositions are observed in Ledig foyaite and inequigranular lujavrite, and contain 0.97−1.37 a.p.f.u. P and 0.90−1.14 a.p.f.u. Sr (Table 4, comp. 8 and 9). This is the most strontian britholite known to date suggesting the existence of a $(Ca_{1-x}Sr_x)_2(LREE,Ca)_3[(Si,P)O_4]_3(PO_4)X$ solid solution, if the $P6_3$ space group of britholite (Oberti *et al.*, 2001) is retained for the Sr-rich variety. Lacking structural data, we cannot rule out ordering of tetrahedrally coordinated cations in this silico-phosphate. However, ordered distribution of both large and small cations, as in *P*3-structured members of the apatite-group such as

TABLE 4. Representative compositions of britholite in postmagmatic assemblages.

	Britholite-I									Britholite-II	
	1	2	3	4	5	6	7	8	9	10	11
Na_2O	–	0.13	–	–	–	0.19	0.26	–	0.83	–	–
CaO	10.07	7.63	8.98	9.04	12.80	15.25	9.50	9.61	10.85	0.38	0.21
SrO	–	0.93	0.83	1.38	0.70	4.71	7.26	11.07	15.66	8.72	9.16
BaO	0.28	–	–	–	–	0.35	–	–	–	0.51	–
MnO	0.33	–	–	0.42	–	0.68	0.06	–	–	1.53	1.57
FeO_t	–	–	–	–	–	1.90	–	0.40	–	1.25	1.53
Ce_2O_3	33.72	40.57	30.65	27.00	33.85	25.60	25.00	29.50	20.74	36.38	35.84
La_2O_3	11.50	22.77	34.97	33.53	20.24	15.36	10.40	9.14	12.33	18.53	17.72
Pr_2O_3	3.77	1.88	1.05	1.31	2.46	1.74	2.35	2.02	1.63	2.53	1.87
Nd_2O_3	12.75	4.25	2.88	2.86	6.17	4.40	17.65	11.13	1.00	8.11	8.98
Sm_2O_3	1.83	–	–	–	–	0.54	1.86	–	–	–	–
Y_2O_3	–	–	–	–	0.55	0.52	0.82	–	–	–	–
P_2O_5	–	–	0.94	0.71	3.27	3.54	5.52	8.18	12.92	0.39	0.18
SiO_2	20.97	21.12	20.19	19.72	19.57	20.44	17.00	14.55	14.15	20.24	20.53
F	2.17	2.04	1.00	0.61	1.14	2.26	2.30	2.28	2.38	1.81	1.25
O=F	−0.91	−0.86	−0.42	−0.26	−0.48	−0.95	−0.97	−0.96	−1.00	−0.76	−0.53
Total	96.64	100.46	101.07	96.32	100.27	97.00	99.01	96.92	100.49	99.62	98.31
Structural formulae calculated on the basis of 8 cations:											
Na	–	0.036	–	–	–	0.047	0.070	–	0.202	–	–
Ca	1.556	1.178	1.359	1.411	1.837	2.071	1.408	1.435	1.460	0.062	0.034
Sr	–	0.078	0.068	0.117	0.054	0.346	0.582	0.895	1.140	0.770	0.811
Ba	0.016	–	–	–	–	0.017	–	–	–	0.030	–
Mn	0.040	–	–	0.052	–	0.073	0.007	–	–	0.197	0.203
Fe_t	–	–	–	–	–	0.201	–	0.047	–	0.159	0.195
La	0.612	1.210	1.822	1.802	1.000	0.718	0.531	0.470	0.571	1.041	0.998
Ce	1.780	2.139	1.585	1.440	1.660	1.188	1.266	1.505	0.953	2.028	2.004
Pr	0.198	0.099	0.054	0.070	0.120	0.080	0.118	0.103	0.075	0.140	0.104
Nd	0.657	0.219	0.145	0.149	0.295	0.199	0.872	0.554	0.448	0.441	0.490
Sm	0.091	–	–	–	–	0.024	0.089	–	–	–	–
Y	–	–	–	–	0.039	0.035	0.060	–	–	–	–
P	–	–	0.112	0.088	0.371	0.380	0.646	0.965	1.373	0.050	0.023
Si	3.024	3.042	2.853	2.873	2.622	2.591	2.351	2.028	1.777	3.081	3.136
LREE	3.337	3.666	3.607	3.460	3.115	2.244	2.936	2.631	2.048	3.650	3.597
F	0.990	0.929	0.447	0.281	0.483	0.906	1.006	1.005	0.945	0.872	0.604
A/T	1.65	1.63	1.70	1.70	1.67	1.67	1.67	1.67	1.54	1.55	1.53
Σ_A	4.95	4.96	5.03	5.04	5.01	5.00	5.00	5.01	4.85	4.87	4.84
Σ_T	3.02	3.04	2.97	2.96	2.99	2.97	3.00	2.99	3.15	3.13	3.16

1−5, 10, 11 replacing eudialyte and *LREE*-rich minerals (rinkite, allanite, *etc.*); 6−9 replacing apatite-group minerals.
1, 2, 4 and 5 in melanolujavrite; 3 and 8 in Ledig foyaite; 6, 10 and 11 in porphyritic lujavrite, 7 and 9 in inequigranular lujavrite

deloneite-(Ce) (Khomyakov *et al.*, 1996; Rastsvetaeva and Khomyakov, 1996) is possible. If so, this phase might have the idealized formula $CaSr(LREE,Ca)_3(SiO_4)_2(PO_4)X$, X = F. Unfortunately, because of the very small size of the crystals and complex intergrowths with other phases, neither X-ray crystal structure determination nor infrared spectroscopic study of this unusual apatite-group phase was possible.

During later high-alkaline post-magmatic stages, britholite-I was subjected to alteration. This is manifested by a patchy appearance of grains in BSE images, and by significant deviations from theoretical stoichiometry,

commonly with P+Si >3 (Table 4, comp. 9), probably resulting from leaching of *A*-site cations.

Britholite-II is more common in melanolujavrite, where it is associated with natrolite replacing analcime. The mineral replaces all the above-described apatite-group minerals, rinkite, allanite, fergusonite and eudialyte. Because of the small grain size, complex intergrowths with other phases, and extensive deuteric alteration, only two reliable britholite-II compositions could be obtained on the larger grains (8 and 12 μm). This phase contains relatively small amounts of F (1.3−1.8 wt.%, or 0.6−0.87 a.p.f.u. F), low to undetectable Ca and P, and up to 3.2 wt.% of MnO and FeO_{tot}. This is enriched in Sr (8−9 wt.% SrO), although to a lesser degree than Brt-I. These compositions are similar to the most strontian britholite from Khibina described by Khomyakov *et al.* (1990), Genkina *et al.* (1991), and Khomyakov (1995). Due to the low total of *A*-cations in britholite-II, the *A*/T ratio is low, and the *LREE* content 'exceeds' the theoretical limit of 3 a.p.f.u.. As the tetrahedral cations in britholite-II also exceed the theoretical limit (T = 3 a.p.f.u.), we consider that such deviations do not arise from coupled tetrahedral substitutions involving low-charge anions, and probably result from leaching of non-lanthanide large cations (Ca, Na, Sr) or the presence of undetermined *LILE* at the *A*-sites.

Discussion

Experiments by Sood and Edgar (1970) showed that the low-pressure solidus of a fluid-rich agpaitic magma capable of producing lujavrite occurs at temperatures close to 450ºC. Interstitial orthomagmatic FAp in Pilansberg nepheline syenite crystallized close to the solidus temperature, and early-post-magmatic Brt-I crystallized slightly below this temperature. Recently, Markl (2001) showed that the nepheline-to-analcime conversion in nepheline syenite takes place in the temperature range 420−200ºC at activity of silica not exceeding 0.1, at activity of water ranging from 1 to 0.5, and correlating antipathetically with activity of silica. These parameters are relevant to the crystallization of FAp-Sr, SrAp and SrAp-*LREE*, as they are coeval with analcime replacing nepheline.

Post-magmatic overprint(s)

Retief (1962) and our studies show that an extensive post-magmatic overprint affected all nepheline syenite units present in the complex and induced re-crystallization, alteration and replacement of all aluminosilicates, eudialyte and most of the accessories. Limited field observations do not indicate the presence of 'foreign' fluids, i.e. development of late-stage hydrothermal veins, mineralized shear zones, compositionally contrasting small intrusions or dykes, etc., thus implying the consanguineous origin of fluids and the autometasomatic character of the post-magmatic processes of the Pilansberg nepheline syenites. As a result of these processes, nepheline, and in some instances alkali feldspar, were successively replaced by sodalite, analcime and ultimately by natrolite. In other instances, alkali feldspar has been converted to ordered triclinic microcline (Mitchell and Liferovich, 2006). Residual nepheline has recrystallized to the Morozewicz-Buerger convergence field (Mitchell and Liferovich, 2004, 2006), thus implying re-equilibration at low-temperatures (Hamilton, 1961), by elimination of excess SiO_2 and Fe_2O_3, the latter giving rise to numerous aegirine microlites in grains of recrystallized nepheline and K-feldspar (Fig. 2*b*,*e*).

A generalized paragenetic sequence for the mineral assemblages in the Pilansberg nepheline syenite, developed from our model for lujavrite (Mitchell and Liferovich, 2004, 2006) is given in Fig. 7. Multistage generation and alteration of 'agpaitic' mineral parageneses with eudialyte and astrophyllite-kupletskite, and of 'miaskitic' mineral parageneses with zircon, pyrochlore and allanite, indicates complex variations in alkalinity during the magmatic and post-magmatic evolution of the Pilansberg nepheline syenite. These modal variations can be explained by autometasomatic processes in a 'nepheline syenite + consanguineous fluid' system as described and modelled by Markl and Baumgartner (2002).

Mineral compositions and textural relationships suggest at least three stages of extensive overprinting by consanguineous fluid which evolved in accordance with the 'alkalinity wave' principle introduced by Khomyakov (1990, 1995) and further modelled and quantified by Markl and Baumgartner (2002). In this model, the pH of a 'deuteric fluid-nepheline syenite' system is controlled by the fluid $a(Na^+)/a(Cl^-)$ ratio. This ratio is influenced by the processes of breakdown/deposition of sodic and chlorine-rich minerals. In the Pilansberg nepheline syenite, alteration of eudialyte-I and sodalite at the early-post-magmatic stage released significant amounts of

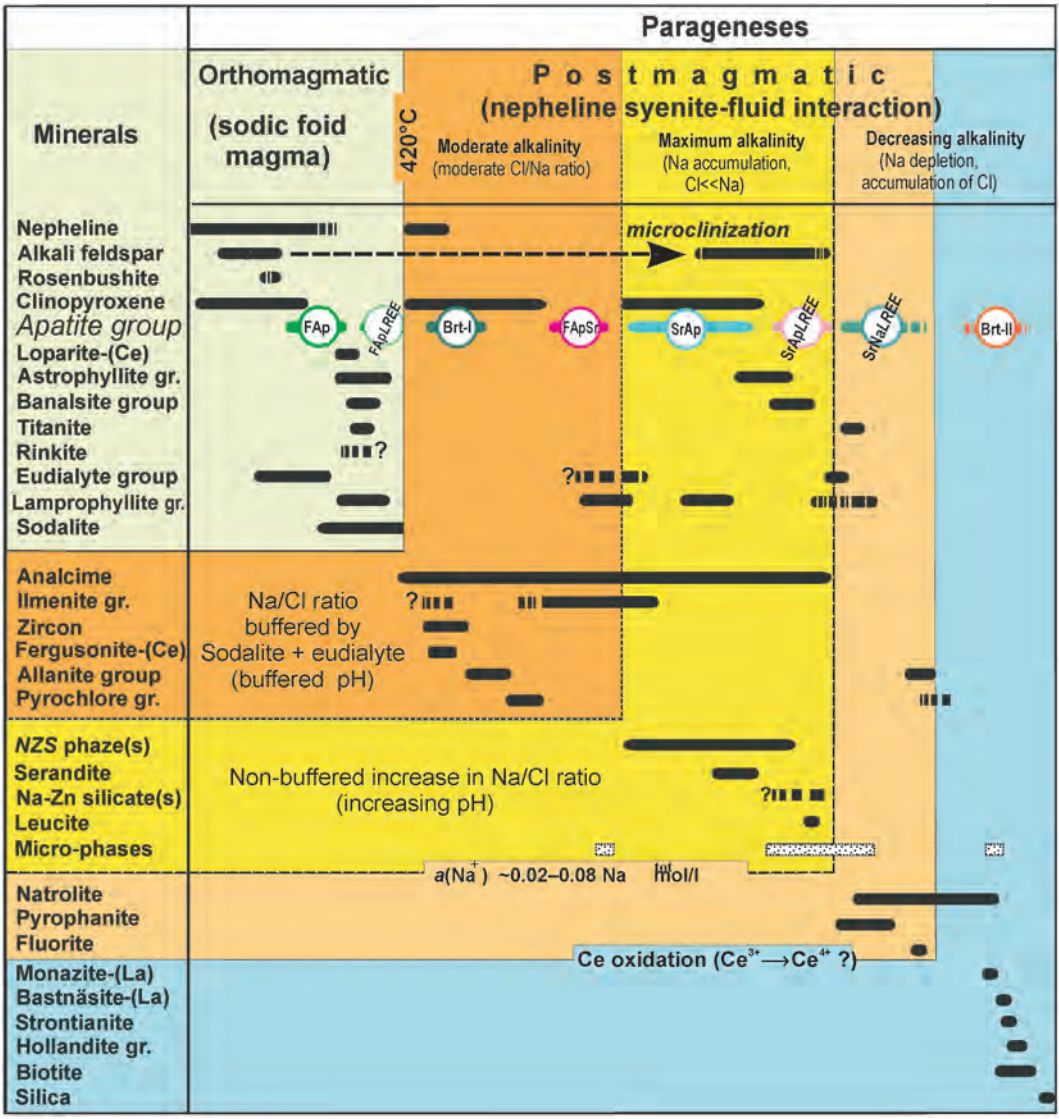

FIG. 7. Generalized sequence of formation of nepheline syenite (lujavrite, white foyaite and Ledig foyaite) in the Pilansberg complex, South Africa. See Markl and Baumgartner (2002) for details of the pH evolution path of sodic fluids.

Cl^- thus decreasing the $a(Na^+)/a(Cl^-)$ ratio, and providing conditions favourable for early-stage 'miaskitic' mineralization (Fig. 7). At the next stage, extensive alteration of nepheline and feldspars resulted in high concentrations of alkalis in the fluid system, and changed the pH to a range characteristic of 'agpaitic-to-hyper-agpaitic' mineralization. The later stages of alteration mark a decrease in $a(Na^+)/a(Cl^-)$ ratio, as substantial amounts of analcime, sodic zirconosilicate(s) and other sodic phases were precipitated and/or replaced nepheline and feldspar. During this stage, and transition to the latest low-temperature stage, recurrent 'agpaitic' mineralization was followed by late-stage 'miaskitic' minerals, both associated with abundant natrolite replacing analcime and nepheline. As the $a(Na^+)/a(Cl^-)$ ratio continued to fall, the lowest-temp-

erature fluids became relatively acidic and deposited fibrous aggregates of silica (Mitchell and Liferovich, 2004, 2006).

Complex compositional evolution of apatite-group minerals and subsolidus alteration of primary fluorapatite are characteristic of evolved agpaitic complexes. Efimov *et al.* (1962), Khomyakov (1995), Pekov *et al.* (1995), and Chakhmouradian *et al.* (2002) have shown that the composition of apatite in sodic and potassic agpaitic rocks of the Inagli, Khibina, Lovozero and Murun peralkaline complexes, evolves from calcian towards strontian compositions (Figs 4, 5) with increasing alkalinity of the deuteric mineral-forming fluids and culminates in crystallization of the 'fluorine-dominant analogue' of Sr-apatite, containing 61–63 wt.% SrO. The latter amount is the empirical limit of Sr-for-Ca substitution in fluorapatite. Data regarding the mineral parageneses of belovite-(Ce), deloneite-(Ce), and fluorcaphite, which are post-magmatic analogues of apatite in agpaitic rocks (Khomyakov, 1995), clearly show that these Sr-Na-*LREE* phosphates are confined to the latest natrolite-rich hydrothermal derivatives of nepheline syenite pegmatites (Pekov *et al.*, 1995, 1996; Khomyakov *et al.*, 1996, 1997; Chakhmouradian *et al.*, 2002). Our observations (Mitchell and Liferovich, 2006) demonstrate that the Sr-Na-*LREE* apatite-group minerals in the Pilansberg nepheline syenite are associated with natrolite and were formed at the stage of decreasing alkalinity, which was followed by 'miaskitic' mineralization. These conclusions are in agreement with the data of Chakhmouradian *et al.* (2005) who described abundant fluorcaphite in a fenite formed from quartzite xenoliths containing albite, pyrochlore, cryptomelane and other minerals typical of low-alkaline ('miaskitic') rocks.

We have observed the sequence 'FAp → Brt-I → FAp-Sr → SrAp → SrAp-*LREE* → Na-Sr-*LREE*-rich apatite-group minerals → Brt-II', in the Pilansberg nepheline syenite (Fig. 7). Evolution of apatite-group minerals from stoichiometric orthomagmatic fluorapatite to post-magmatic Sr-, Na-Sr-*LREE* and Si-*LREE* analogues in the Pilansberg nepheline syenites is similar to that described for other feldspathoidal rocks, their pegmatites and post-magmatic derivatives (Efimov *et al.*, 1962; Khomyakov, 1995; Chakhmouradian and Mitchell, 1999, 2002; Chakhmouradian *et al.*, 2002, 2005). Regardless of the similarities, the apatite-group minerals in Pilansberg nepheline syenites demonstrate unique features of compositional evolution governed by the complex *in situ* variations of alkalinity of the mineral-forming fluids enriched in Sr, Na, *LREE*, and finally saturated in Si. Thus, several generations of the apatite-group minerals coexist on a hand-specimen size scale in contrast to other nepheline syenite complexes, where the most evolved compositions occur in pegmatites or zeolite-rich veins. To our knowledge, FAp, FAp-Sr are common in nepheline syenites with FAp-Sr, SrAp and SrAp-*LREE* usually being found in evolved nepheline syenite pegmatite segregations with zeolite-rich axial zones and cores. The latest zeolite veins conjugate with these rocks are known to contain SrAp, SrAp-*LREE*, as well as fluorcaphite, belovite and deloneite, the Na-Sr-*LREE*-rich analogues of apatite. Britholite-(Ce) and the Na-Sr-*LREE*-rich analogues of apatite have been previously reported from fenites and hybrid rocks (Kostyleva-Labuntsova *et al.*, 1978; Chakhmouradian *et al.*, 2005). In contrast, all apatite-group minerals, including the two generations of britholite, are disseminated as abundant accessories in Pilansberg nepheline syenite. Unlike most other agpaitic complexes, the deuteric fluid phase consanguineous with Pilansberg nepheline syenite has been retained *in situ* and apparently did not separate into discrete pegmatite bodies and hydrothermal veins.

Our observations provide further support for the empirical observations of Khomyakov (1990, 1995) and Chakhmouradian *et al.* (2002) regarding the strong positive correlation between the Sr enrichment of apatite and alkalinity. In the Pilansberg nepheline syenite, apatite *sensu stricto* becomes unstable under high-alkaline conditions and is replaced initially by Sr- and subsequently by Sr-Na-*LREE* analogues. Our data also agree well with the conclusions of Chakhmouradian *et al.* (2002) regarding the naturally occurring continuous $Ca_{10-x}Sr_x(PO_4)_6X$ solid solution series. The most strontian apatite observed in Pilansberg, contains 62.1 wt.% SrO and only 6.1 wt.% CaO, i.e. similar to the maximum concentration reported for Sr in apatite described recently as a product of deuteric reactions of fluorapatite in nepheline syenite pegmatites at Lovozero (Pekov, 2001; Chakhmouradian *et al.*, 2002). In all cases, the most Sr-rich samples of natural apatite contain 61.3–62.9 wt.% SrO (4.22–4.54 a.p.f.u. Sr). The most strontian compositions observed in the Pilansberg nepheline syenite correspond to ~83–85 mol.% of the theoretical $Sr_5(PO_4)_3F$ end-member and

~13 mol.% of fluorapatite *sensu stricto*. These compositions are identical to those described for a deuteric Sr-apatite by Pekov (2001). The Sr-apatite with ~91 mol.% $Sr_5(PO_4)_3F$ described by Chakhmouradian *et al.* (2002) might be overestimated, as their composition, which had an analytical total of ~97 wt.%, contained only 2.6 wt.% CaO, and did not exhibit significant deficiency of tetrahedral cations and fluorine (2.99 and 0.95 a.p.f.u., respectively).

Some of the observed compositional features of apatite-group minerals in the Pilansberg nepheline syenite have not been described previously and imply the existence of new substitutional schemes and solid-solution series. Although speculative, due to the absence of structural data, we suggest these are:

(1) A complex $(Na_{2-x}Ca_x)(Ca,Sr)(LREE,Sr)Sr_2(PO_4)_6(F,OH)$ solid-solution series, with a possible join to $CaLREESr_3(PO_4)_6F$ for Sr-Na-*LREE* fluorapatite formed during the stage of decreasing alkalinity in paragenesis with recurrent 'agpaitic mineral assemblages'.

(2) A complex series between belovite-(Ce), $NaCeSr_3(PO_4)_3F$, and strontian britholite-(Ce), $(Ca_{1-x}Sr_x)_2LREE_3[(Si_{1-y}P_y]O_4)_3F$, produced by subsolidus replacement of Sr-Na-*LREE* apatite in contact with deuteric fluids.

(3) A solid-solution series between britholite-(Ce) and strontian britholite-(Ce), $(Ca_{1-x}Sr_x)_2(LREE,Ca)_3[(Si,P)O_4]_3(PO_4)F$, formed by deuteric alteration of Sr-rich apatite-group minerals.

Conclusions

Pilansberg nepheline syenites have undergone extensive subsolidus equilibration with a consanguineous deuteric Cl- and Na-rich fluid phase. Complex assemblages of secondary minerals have replaced the primary aluminosilicates, rinkite, eudialyte and fluorapatite. Three types of alteration and replacement of fluorapatite have been recognized and the mineral assemblages formed are considered to reflect the Na/Cl ratio and pH of the deuteric fluids the composition of which changes continuously as a result of extensive interactions with both primary and secondary minerals. The latter, in sequence, range from a primary agpaitic to early miaskitic assemblage, through post-magmatic agpaitic and hyperagpaitic types, with a return to low agpaitic and miaskitic assemblages in the final stages of alteration. Variations of cationic composition of apatite-group minerals are sensitive indicators of evolution of the mineral-forming fluids in the course of autometasomatic alteration of Pilansberg nepheline syenite. Increasing alkalinity is indicated by increasing amounts of Sr replacing Ca. Significant amounts of Na, *LREE* and Sr are sequestered in apatite at the stage of decreasing alkalinity. Both high- and low-temperature low-alkaline fluids produced strontian britholite-(Ce), including a siliceous end-member. The Pilansberg apatite-group minerals form a near complete solid solution between fluorapatite and a 'fluorine analogue' of Sr-apatite, together with a limited solid-solution series towards belovite, an unusual Si-rich belovite-(Ce) and strontian britholite-(Ce).

Acknowledgements

This work is supported by the Natural Sciences and Engineering Research Council of Canada and Lakehead University (Canada). We thank Anne Hammond for sample preparation. Alexander Podlesny is cordially thanked for donating the minerals employed for analytical quality control. Dr R.C. (Jock) Harmer is thanked for assistance with collection of Pilansberg syenite. The Director of the Pilansberg National Park is thanked for permission to undertake geological investigations in the Park area. The comments by two referees, Drs G. Markl and I. Broska, as well as by Associate Editor Dr P. Hoskin, are much appreciated.

References

Arden, K.M. and Halden, N.M. (1999) Crystallization and alteration history of britholite in rare-earth-element-enriched pegmatitic segregations associated with the Eden Lake complex, Manitoba, Canada. *The Canadian Mineralogist*, **37**, 1239–1253.

Chakhmouradian, A.R. and Mitchell, R.H. (1999) Primary, agpaitic and deuteric stages in the evolution of accessory Sr, REE, Ba and Nb-mineralization in nepheline-syenite pegmatites at Pegmatite Peak, Bearpaw Mts., Montana. *Mineralogy and Petrology*, **67**, 85–110.

Chakhmouradian, A.R. and Mitchell, R.H. (2002) The mineralogy of Ba- and Zr-rich pegmatites from Gordon Butte, Crazy Mountains (Montana, USA): comparison between potassic and sodic agpaitic pegmatites. *Contributions to Mineralogy and Petrology*, **143**, 93–114.

Chakhmouradian, A.R., Reguir, E.P. and Mitchell, R.H. (2002) Strontium-apatite: new occurrences, and the extent of Sr-for-Ca substitution in apatite-group

minerals. *The Canadian Mineralogist*, **40**, 121–136.

Chakhmouradian, A.R., Hughes, J.M. and Rakovan, J. (2005) Fluorcaphite, a second occurrence and detailed structural analysis: simultaneous accommodation of Ca, Sr, Na and *LREE* in the apatite atomic arrangement. *The Canadian Mineralogist*, **43**, 735–746.

Efimov, A.F., Kravchenko, S.M. and Vasil'eva, Z.V. (1962) Strontium-apatite – a new mineral. *Doklady Academii Nauk USSR, Earth Science Section*, **142**, 113–116 (in Russian).

Ferguson, J. (1973) The Pilansberg alkaline province. *Transactions of the Geological Society of South Africa*, **376**, 207–214.

Féménias, O., Coussaert, N., Brassinnes, S. and Demaiffe, D. (2005) Emplacement processes and cooling history of layered cyclic unit II-7 from the Lovozero alkaline massif (Kola peninsula, Russia). *Lithos*, **83**, 371–393.

Genkina, E.A., Malinovskii, Yu.A. and Khomyakov, A.P. (1991) Crystal structure of Sr-containing britholite. *Soviet Physics Crystallography*, **36**, 19–22.

Hamilton, D.L. (1961) Nepheline as crystallization temperature indicators. *Journal of Geology*, **69**, 321–329.

Khomyakov, A.P. (1990) Mineralogy of hyperagpaitic alkaline rocks. Moscow, *Nauka*, 195 pp. (in Russian).

Khomyakov, A.P. (1995) *Mineralogy of Hyperagpaitic Alkaline Rocks*. Oxford Science, 223 pp.

Khomyakov, A.P., Spachenko, A.K. and Polezhaeva, L.I. (1990) Melilite and rare earth phosphate mineralization at the Namuaiv Mount (Khibina). Pp. 106–119 in: *Alkaline Magmatism in the NE part of the Baltic Shield* (T.N. Ivanova, O.B. Dudkin and A.A. Arzamastsev, editors). Kola Science Centre RAS, Apatity, Russia (in Russian).

Khomyakov, A.P., Lisitsyn, D.V., Kulikova, I.M. and Rastsvetaeva, R.K. (1996) Deloneite-(Ce), $NaCa_2SrCe(PO_4)_3F$ – a new mineral with a belovite-like structure. *Zapiski Vserossiiskogo Mineralogicheskogo Obshchestva*, **125(5)**, 83–94 (in Russian).

Khomyakov, A.P., Kulikova, I.M. and Rastsvetaeva, R.K. (1997) Fluorcaphite $Ca(Sr,Na,Ca)(Ca,Sr,Ce)_3(PO_4)_3F$ – a new mineral with an apatite-like structural motif. *Zapiski Vserossiiskogo Mineralogicheskogo Obshchestva*, **126(3)**, 87–97 (in Russian).

Kostyleva-Labuntsova, E.E., Borutsky, B.E., Sokolova, M.N., Shlyukova, Z.V., Dorfman, M.D., Dudkin, O.B. and Kozyreva, L.V. (1978) *Mineralogy of Khibina Complex, part II*. Nauka, Moscow, 585 pp. (in Russian).

Lurie, J. (1986) Mineralization of the Pilansberg Alkaline Complex. Pp. 2215–2228 in: *Mineral Deposits of South Africa* **2** (C.R. Anhaeusser, and S. Maske, editors). The Geological Society of South Africa, Johannesburg, South Africa.

Mandarino, J.A. (1999) *Fleisher's Glossary of Mineral Species*. The Mineralogical Record Inc., Tucson, Arizona, 225 pp.

Markl, G. (2001) A new type of silicate liquid immiscibility in peralkaline nepheline syenites (lujavrites) of the Ilímaussaq complex, South Greenland. *Contributions to Mineralogy and Petrology*, **141**, 458–472.

Markl, G. and Baumgartner, L. (2002) pH changes in peralkaline late-magmatic fluids. *Contributions to Mineralogy and Petrology*, **144**, 331–346.

Mitchell, R.H. and Belton, F. (2004) Niocalite-cuspidine solid solution and manganoan monticellite from natrocarbonatite, Oldoinyo Lengai, Tanzania. *Mineralogical Magazine*, **68**, 787–799.

Mitchell, R.H. and Liferovich, R.P. (2004) Ecandrewsite-zincian pyrophanite from lujavrite, Pilansberg alkaline complex, South Africa. *The Canadian Mineralogist*, **42**, 1169–1178.

Mitchell, R.H. and Liferovich R.P. (2005) Subsolidus/deuteric alteration of eudialyte in aegirine lujavrite, Pilansberg Alkaline Complex, South Africa. Pp. 74–76 in: *Peralkaline Rocks: Sources, Economic Potential and Evolution from Alkaline Melts* (M. Marks, editor). PERALK Workshop, Abstract volume, Tübingen, Germany.

Mitchell, R.H. and Liferovich, R.P. (2006) Subsolidus deuteric/hydrothermal alteration of eudialyte in lujavrite from the Pilansberg Alkaline Complex, South Africa. *Lithos*, **91**, 352–372.

Mitchell, R.H. and Vladykin, N.V. (1993) Rare earth element-bearing tausonite and potassium barium titanates from the Little Murun potassic alkaline complex, Yakutia. *Mineralogical Magazine*, **57**, 651–664

Nadezhina, T.N., Pushcharovsky, D.Yu. and Khomyakov, A.P. (1987) Refinement of crystal structure of belovite. *Mineralogical Zhurnal*, **9**(2), 45–48 (in Russian).

Oberti, R., Ottolini, L., Della Ventura, G. and Parodi, G.C. (2001) On the symmetry and crystal chemistry of britholite: New structural and microanalytical data. *American Mineralogist*, **86**, 1066–1075.

Olivo, G.R. and Williams-Jones, A.E. (1999) Hydrothermal *REE*-rich eudialyte from the Pilansberg complex, South Africa. *The Canadian Mineralogist*, **38**, 653–663.

Pan, Yu. and Fleet, M. (2002) Compositions of apatite-group minerals: substitution mechanisms and controlling factors. Pp. 13–49 in: *Phosphates – Geochemical, Geological, and Materials Importance* (M.J. Kohn, J. Rakovan and J.M.

Hughes, editors). Reviews in Mineralogy and Geochemistry, **48**. Mineralogical Society of American and the Geochemical Society, Washington, D.C.

Pekov, I.V. (2001) *Lovozero Massif: History of Investigations, Pegmatites, Minerals*. Zemlya Press, Moscow, 432 pp. (in Russian).

Pekov, I.V., Chukanov, N.V., Eletskaya, O.V., Khomyakov, A.P. and Menshikov, Yu.P. (1995) Belovite-(Ce): new data, refined formula, and relationships with other minerals of apatite group. *Zapiski Vserossiiskogo Mineralogicheskogo Obshchestva*, **124(2)**, 98–110 (in Russian).

Pekov, I.V., Kulikova, I.M., Kabalov, Yu.K., Eletskaya, O.V., Chukanov, N.V., Menshikov, Yu.P. and Khomyakov, A.P. (1996) Belovite-(La), $Sr_3Na(La,Ce)[PO_4]_3(F,OH)$ – a new rare earth mineral of the apatite group. *Zapiski Vserossiiskogo Mineralogicheskogo Obshchestva*, **125(3)**, 101–109 (in Russian).

Pushcharovsky, D.Yu., Nadezhina, T.N. and Khomyakov, A.P. (1987) Crystal structure of strontium-apatite from Khibina. *Crystallography Reports*, **32**, 891–895 (in Russian).

Rakovan, J.F. and Hughes, J.M. (2000) Strontium in the apatite structure: strontian fluorapatite and belovite-(Ce). *The Canadian Mineralogist*, **38**, 839–845.

Ramsay, W. (1890) Geologische Beobachtuntgen auf der Halbinsel Kola. Nebst einem Anhange: Petrographische Beschreibung der Gesteine des Lujavr-urt. *Fennia*, III, **7**, 1–52 (in German).

Rastsvetaeva, R.K. and Khomyakov, A.P. (1996) Crystal structure of deloneite-(Ce), a highly ordered Ca-analogue of belovite. *Doklady Rossiyskoi Akademii Nauk*, **349**, 354–357 (in Russian).

Retief, E.A. (1962) Preliminary observations on the feldspars from the Pilanesberg alkaline complex, Transvaal, S. Africa. *Norsk Geologisk Tidsskrift*, **42(2)**, 493–513.

Retief, E.A. (1963) *Petrological and mineralogical studies in the southern part of the Pilansberg Complex, Transvaal, South Africa*. PhD thesis, Oxford University, Oxford, UK.

Rønsbo, J.G. (1989) Coupled substitutions involving *REE*s and Na and Si in apatites in alkaline rocks from Ilímaussaq intrusion, South Greenland, and the petrological implications. *American Mineralogist*, **74**, 896–901.

Shand, S.I. (1928) The geology of Pilansberg in the Western Transvaal. *Transactions of Geological Society of South Africa*, **31**, 91–156.

Sood, M.K. and Edgar, A.D. (1970) Melting relations of undersaturated alkaline rocks. *Meddelelser om Grønland*, 181 pp.

Stormer, J.C., Pierson, M.L. and Tacker, R.C. (1993) Variation of F and Cl X-ray intensity due to anisotropic diffusion in apatite during electron microprobe analysis. *American Mineralogist*, **78**, 641–648.

Zaitsev A.N. and Chakhmouradian, A.R. (2002) Calcite-amphibole-clinopyroxene rock from the Afrikanda complex, Kola peninsula, Russia: mineralogy and possible link to carbonatites. II. Oxysalt minerals. *The Canadian Mineralogist*, **40**, 103–120.

[*Manuscript received 3 January 2006: revised 20 October 2006*]